SANDIA REPORT

SAND2012-7803
Unlimited Release
Printed September 2012

The Mechanics of Network Polymers with Thermally Reversible Linkages

Kevin N. Long

Prepared by
Sandia National Laboratories
Albuquerque, New Mexico 87185 and Livermore, California 94550

Sandia National Laboratories is a multi-program laboratory managed and operated by Sandia Corporation, a wholly owned subsidiary of Lockheed Martin Corporation, for the U.S. Department of Energy's National Nuclear Security Administration under contract DE-AC04-94AL85000.

Approved for public release; further dissemination unlimited.

Sandia National Laboratories

Issued by Sandia National Laboratories, operated for the United States Department of Energy by Sandia Corporation.

NOTICE: This report was prepared as an account of work sponsored by an agency of the United States Government. Neither the United States Government, nor any agency thereof, nor any of their employees, nor any of their contractors, subcontractors, or their employees, make any warranty, express or implied, or assume any legal liability or responsibility for the accuracy, completeness, or usefulness of any information, apparatus, product, or process disclosed, or represent that its use would not infringe privately owned rights. Reference herein to any specific commercial product, process, or service by trade name, trademark, manufacturer, or otherwise, does not necessarily constitute or imply its endorsement, recommendation, or favoring by the United States Government, any agency thereof, or any of their contractors or subcontractors. The views and opinions expressed herein do not necessarily state or reflect those of the United States Government, any agency thereof, or any of their contractors.

Printed in the United States of America. This report has been reproduced directly from the best available copy.

Available to DOE and DOE contractors from
U.S. Department of Energy
Office of Scientific and Technical Information
P.O. Box 62
Oak Ridge, TN 37831

Telephone: (865) 576-8401
Facsimile: (865) 576-5728
E-Mail: reports@adonis.osti.gov
Online ordering: http://www.osti.gov/bridge

Available to the public from
U.S. Department of Commerce
National Technical Information Service
5285 Port Royal Rd
Springfield, VA 22161

Telephone: (800) 553-6847
Facsimile: (703) 605-6900
E-Mail: orders@ntis.fedworld.gov
Online ordering: http://www.ntis.gov/help/ordermethods.asp?loc=7-4-0#online

SAND2012-7803
Unlimited Release
Printed September 2012

The Mechanics of Network Polymers with Thermally Reversible Linkages

Kevin N. Long
Solid Mechanics Department
Sandia National Laboratories
P.O. Box 5800
Albuquerque, NM 87185-9999
knlong@sandia.gov

Abstract

Encapsulated printed circuit boards typically use conventional thermosetting polymers which are difficult to remove without damaging the electronics if upgrades are needed. To improve the efficiency of maintaining printed circuit boards, network polymers with thermally reversible linkages were developed to provide an alternative class of encapsulation thermosets that could be easily and non-destructively removed and later reapplied. These polymers include functionalities that dynamically break and form covalent bonds. Over time, the connectivity of the network evolves, which causes the macroscopic stress in the material to relax and the permanent shape to change even if these processes are in equilibrium. With respect to removal, the equilibrium behavior of these processes changes if the thermodynamic state of the material is changed, which alters the number density of chains. If the number density of chains is reduced below the percolation threshold, the material exhibits a gel-point transition beyond which, it behaves as a viscous liquid. These two properties contrast sharply with conventional thermosetting polymers, which do not exhibit this relaxation mechanism nor a gel-point transition.

To take advantage of such novel material capabilities at length scales relevant to electronics packaging, a continuum-scale constitutive model is needed that correctly accounts for the thermal-chemical-viscoelastic behavior of such materials, especially since the state of the art for using them is limited to experimental investigations. To meet this need, a continuum-scale, thermodynamically consistent free energy description of such materials is developed in this work. Paired with this free energy are non-equilibrium contributions associated with the topological rearrangement of the network as chains are added and removed as well as viscoelasticity. The model is calibrated and validated against experimental data published in the literature. Finally, simple encapsulation thermal-mechanical scenarios are examined that demonstrate a substantial difference in behavior between conventional polymer networks vs. those with thermally reversible linkages.

Acknowledgment

This research was supported by the Early Career Laboratory Directed Research and Development program at Sandia National Laboratories. The author is grateful for the many important discussions with William Scherzinger, David Wheeler, James Aubert, and Robert Chambers that helped shape this work.

Contents

1 **Introduction** **11**

2 **Experimental Observations** **15**

3 **Constitutive Model Development** **17**

Kinematics 17

Mass, Species, and Momentum Balances 18

Energy Balance 19

Entropy Production Inequality 20

Equation of Motion for the Temperature Field 22

Species and Thermal Energy Transport 23

Diels-Alder Chemistry 24

Diels-Alder Reaction Kinetics 26

Shear Modulus Dependence on the Chemical Species 27

Evolution of the Stress-Free Configuration 28

Additive Split of the Helmholtz Free Energy Density 30

Equilibrium Free Energy Contributions 31

Non-Equilibrium Helmholtz Free Energy Contributions 32

Model Parameters and Experiments Necessary to Populate Them 35

4 **Results** **39**

Analytic Solutions of Rubbery Removable Encapsulation 39

Model Calibration and Validation 43

Removable Thermosets in Underfill Scenarios 45

5 Conclusions **51**

References **52**

List of Figures

1.1 Dynamic covalent linkages 11

1.2 Schematic of representative volume elements of a polymer network above and below the percolation threshold network connectivity. 12

1.3 Non-destructive thermoset foam removal from [14] 13

1.4 Demonstration of underfill thermal mismatch strain failing solder joints on printed circuit boards 14

2.1 Temperature dependence of the Diels-Alder chemical equilibrium and adduct chemical half-life 16

4.1 Analytic solution: isothermal rubbery removable network polymer stress relaxation 41

4.2 Analytic solution: isothermal rubbery removable network polymer uniaxial extension at a fixed strain rate 42

4.3 Dynamic mechanical analysis validation 44

4.4 Applied temperature history thermal-mechanical cycle 46

4.5 Single element thermal-mechanical cycle: $\Theta_{glass} = \Theta_{min}$ 48

4.6 Single element thermal-mechanical cycle: $\Theta_{glass} = \Theta_{mid}$ 49

List of Tables

3.1 Properties of the Diels-Alder chemistry and transport 36

3.2 Equilibrium helmholtz free energy density parameters. 37

3.3 Non-equilibrium helmholtz free energy density parameters. 38

4.1 Calibrated material properties associated with the dynamic mechanical analysis validation predictions. Quantities are taken directly from reference [6] with the exception of K^{∞} and β^{∞}, which were chosen as discussed in the text. 43

4.2 Model properties used to compare the thermal-mechanical behavior of removable vs. non-removable thermosets in underfill scenarios. 47

Chapter 1

Introduction

Network polymers with thermally reversible functionalities are atypical thermosets. A snapshot of the macromolecule would appear typical; chains are joined at covalent chemical cross-links as well as physically entangled through Van-der-Waals interactions. However, specific functionalities have been included along their polymer chains and cross-linking sites, and these functionalities undergo thermally stimulated, reversible chemical reactions that connect or disconnect chains from the network [15, 37, 34]. An actively explored chemistry in the literature integrates furan and maleimide functionalities that undergo the highly reversible, Diels-Alder (DA) cycloaddition reaction along polymer chains and at cross-linking sites [24, 33, 6, 26, 32]. In such networks, these functional groups behave as dynamic bonds that break and reform over time. A cartoon of this process with tri-furan and bis-maleimide functionalities is shown in Fig. 1.1. This DA chemistry occurs through the cycloaddition reaction of furan and maleimide species. If a sufficient number of chains are broken such that no single chain spans the material, then the polymer network has crossed the percolation threshold (gel-point). In this state, the polymer is no longer a network, and it behaves as a liquid and can be removed. A schematic of such connectivities is presented

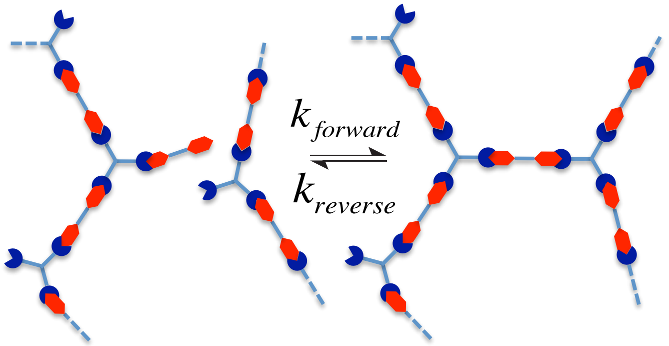

Figure 1.1. Dynamic covalent linkages break and reform in a reversible manner, which provides the polymer network an intrinsic mechanism to change its topology and permanent shape. The complementary red and blue shapes respectively represent bis-maleimide and tri-furan functionalities that undergo the reversible, Diels-Alder reaction. The dashed lines indicate chains continuing into the rest of the network.

above and below the gel point. ‘ Under thermodynamic equilibrium conditions (chemical equilibrium, thermal equilibrium, etc.), the aggregate connectivity of the network is static, even while the chains themselves dynamically break and reform. The effect is that the network topology evolves over time, and when such materials are subjected to mechanical stresses, relaxation is observed, and the permanent shape of the material evolves [24, 10, 6, 32]. Another important effect is that the network has a thermally tunable set of cross-links and therefore, a thermally tunable number density of chains, which arises due to the temperature dependence of the Diels-Alder chemical equilibrium. And this phenomenon occurs even if another, permanent set of cross-links is present in the network.

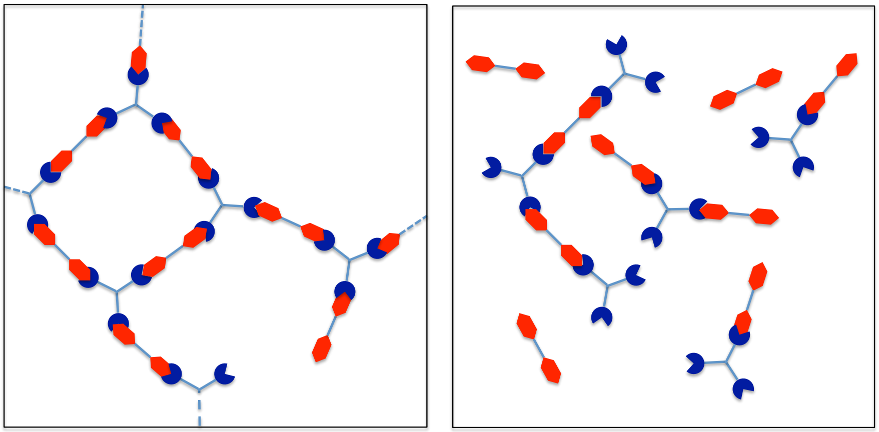

(a) Polymer chains beyond the percolation threshold (not removable) **(b)** Polymer chains below the percolation threshold (removable)

Figure 1.2. Schematic of representative volume elements (black boxes) of a polymer network above and below the percolation threshold network connectivity which controls whether the material can be removed.

The chemical literature has seen considerable activity in this area associated with ”clique chemistry” [15]. Chemists have identified the paradigm that reversible linkages can be incorporated into the network that can be stimulated by temperature [7, 10] and light [30, 17]. A critical feature distinguishes these two stimuli. In the case of photo-chemically induced network topology evolution, the stimulus can be shut-off (turn off of the light source). However, for reversible thermal chemistries, the process can only be slowed by adjusting the temperature. A variety of applications have been proposed from thermoset recycling [25], self healing materials [37, 23, 20, 7, 10], and novel sensors and actuators [16, 29, 21].

Network polymers with thermally reversible functionalities were developed at Sandia National Laboratories to respond to a specific business need for non-destructive, removable thermosetting encapsulation of electronics [24]. This novel material capability allows for the thermoset encapsulation to be removed above a critical temperature or at a reduced temperature in the presence of a solvent, and hence we label such materials as removable network polymers (RNP). Both rubbery and glassy behaviors may be required depending on the encapsulation need, and so thermoplastic encapsulation cannot be used. RNPs were formulated to have desired thermal-mechanical properties (T_{glass}, moduli, thermal expansion behavior, etc.) and included DA functionalities for removability above a critical temperature. For example, MacElhanon and co-workers demonstrated the non-destructive removal of a conforming RNP foam about an electrical component. These materials and associated applications involve multiple physical processes subjected to large deformations. The combination of which would be difficult to optimize experimentally. To realize such sophisticated applications, theoretical and computational design tools are needed. The objective of this paper is to meet this engineering need through the development of a thermal-chemical-mechanical constitutive model. Two predictive features of the model are desirable:

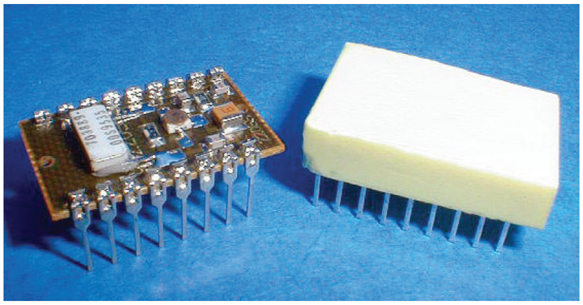

Figure 1.3. Non-destructive, non-mechanical removal of a conformal RNP foam [14] reprinted with permission from Sandia National Laboratories.

- Simulating the process of removing the RNP encapsulation
- Simulating the complex thermal-chemical-mechanical behavior during the service lifetime of the encapsulation

In the context of bullet one, experimental demonstration and characterization, such as in Fig. 1.3, may sufficiently inform design engineers on how to non-destructively remove RNP encapsulation from electronics. However, without the capability to perform bullet two, one cannot predictively quantity the different thermal-mechanical behavior that RNP encapsulation will exhibit compared with traditional (non-removable) thermosetting encapsulation, which is anticipated given the inherent stress relaxation mechanism that the thermally-reversible functionalities provide in the RNP. Such predictive capabilities become especially important when considering the effects of thermal mismatch strains between the polymer and other components on printed circuit. Specifically, polymer underfills can cause solder join fatigue and failure of components subjected to thermal cycling [2]. For example, as shown in Fig. 2.1, solder joints of underfilled components may fatigue and eventually fail due to the thermal-expansion mismatch between the solder and the polymer encapsulation.

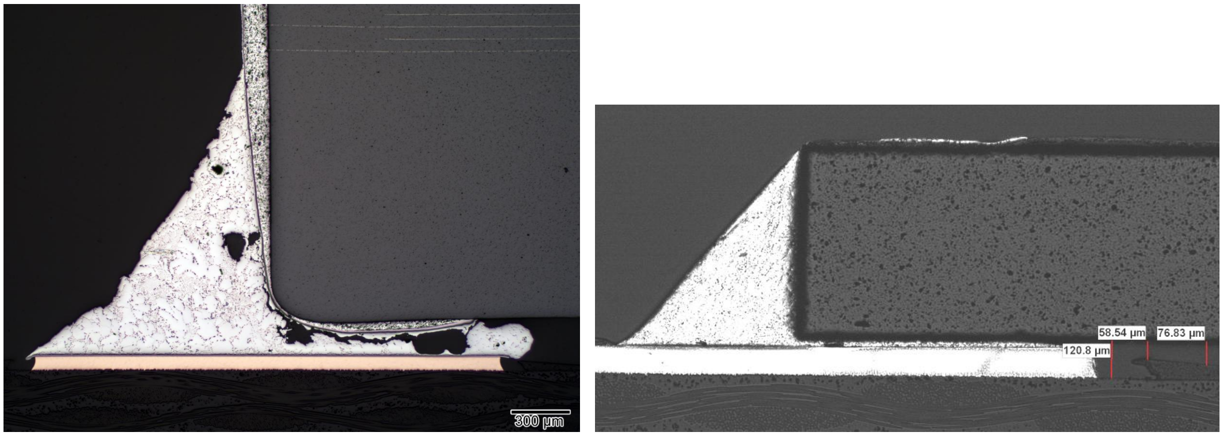

(a) Cross-sectioned cracked solder joint, ”large” capacitor, and a traditional epoxy underfill in its glassy state

(b) Cross-sectioned in-tact solder joint, ”small” capacitor, and a traditional epoxy underfill in its glassy state

Figure 1.4. Traditional network polymer underfill encapsulation may fail solder joints on printed circuit boards due to thermal mismatch strain and geometric considerations. If a removable network polymer underfill enapsulant is used, then its relaxation behavior may change the thermal mismatch strain that stresses the solder joints, and thus this additional behavior must be considered. Figures are taken from [2] and reprinted with permission from Sandia National Laboratories.

To meet this predictive capability need, we develop a thermodynamically consistent, continuum scale constitutive model, validate it against limited data in the literature, and use it to examine the distinct behavior of RNPs in simple underfill encapsulation scenarios.

The article is laid out as follows. First, we select a model experimental system from the literature and discuss basic experimental observations in the context of the Diels-Alder chemistry, network topology evolution, and associated stress relaxation. Next, we develop the thermal-chemical-mechanical constitutive model and the associated kinetics of the chemistry, glassy behavior, and evolution of the permanent shape due to changes in the network topology. The specific forms of the balance laws that govern its behavior are also presented. We then examine special cases of the model behavior that admit semi-analytic solutions, present validation results of the model against limited experimental data, and finally compare the behavior of removable vs. traditional encapsulation materials under simple thermal-mechanical cycling.

Chapter 2

Experimental Observations

We briefly discussing experimental results developed by Bowman and co-workers [6] that guide theoretical and validation efforts in this paper. They form a network which is cross-linked with tri-furan and bismaleimide functionalities capable of undergoing the (retro-)Diels-Alder (DA) reaction. Specifically, they copolymerize Pentaerythritol Propoxylate Tris(3-(furfurylthiol)- propionate) (PPTF) and 1,1'- (methylenedi-4,1-phenylene) bismaleimide (DPBM) by mixing them in a 1:1 furan to maleimide ratio, heating the mixture for 5 minutes at 155 C to complete the step-growth reaction, and then cooling the material to room temperature. They observed a solid material that visibly reverted to a liquid above 110C and vitrified below 45C. The furan and maleimide functionalities are analogous to the two different geometric symbols in Fig. 1.2 and may reversibly bond together to form a Diels-Alder adduct.

Using Fourier Transform Infrared Spectroscopy (FTIR), Bowman and co-workers, measured the equilibrium extent of reaction as a function of temperature, which is defined as the adduct concentration normalized to its maximum possible concentration (assuming all species are bonded). The equilibrium extent of reaction vs. temperature is reproduced here. They additionally measured both the forward and reverse reaction kinetics and fit their respective behaviors following a simple, single reaction step, thermal-chemical reaction kinetics. Using their calibrated thermal-chemical kinetic results, we calculate the half-life a DA adduct, which characterizes both the equilibrium and non-equilibrium rate at which DA linkages in the network break (and, in equilibrium, reform). Hence, this chemical half-life controls the rate at which the permanent shape of the material evolves in the absence of vitrification. The advantage of using this system over more complicated DA thermoset chemistries formulated with multiple cross-linking species is that the polymer structure and dynamics are simpler since these other explored systems involve both permanent and reversible cross-links. The key experimental observations that we wish to capture through the development of a thermal-chemical-mechanical constitutive equation are:

- The dependence of the material's permanent shape change (network topology evolution) on the DA chemical kinetics
- The relationship between the rubbery shear modulus and the extent of the DA reaction
- Thermodynamic properties
- Glassy behavior

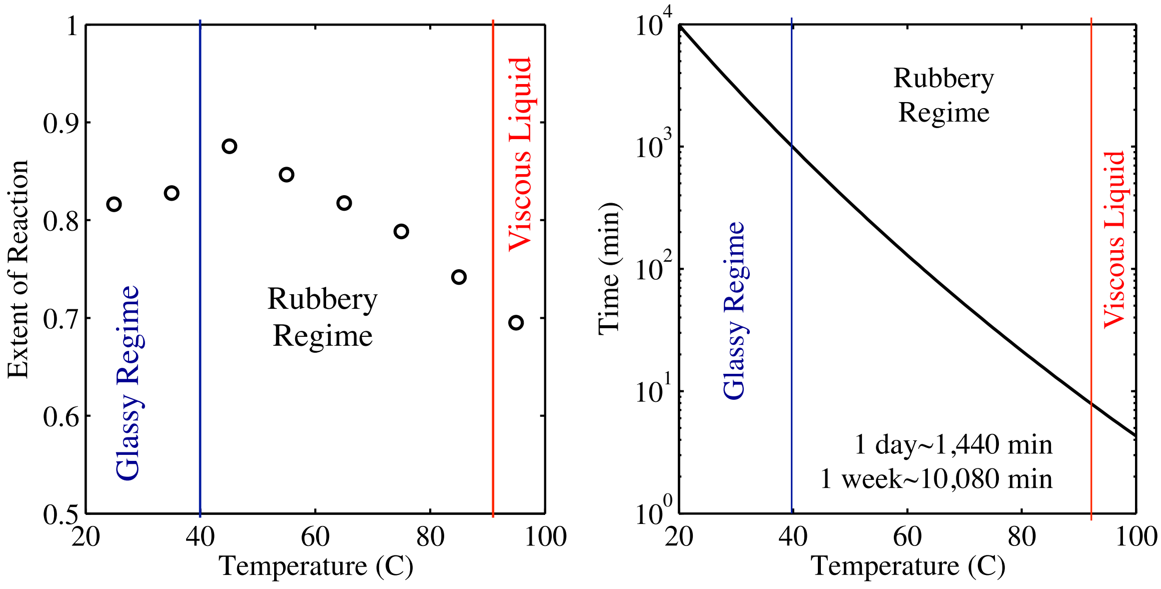

(a) Equilibrium extent of the Diels-Alder Reaction **(b)** Chemical half-life of a Diels-Alder adduct

Figure 2.1. The equilibrium extent of reaction (with the exception of points below the glass transition) and the chemical half-life of a bonded Diels-Alder linkage. The data is partially reproduced from reference [6]. Note that even at room temperature, half of the linkages will break and reform within a week!

Chapter 3

Constitutive Model Development

We seek to develop a constitutive model for network polymers with thermally reversible linkages in a continuum setting. The purpose of this model is to inform the use of such materials in electronics packaging. Since the network topological rearrangement occurs at a length scale smaller than that of encapsulation, which is our main application driver, we consider our continuum approach reasonable and model the bulk behavior of the material. We develop the model in the following order. We briefly discuss kinematics including non-traditional invariants later used in the free energy developments, and then we summarize the mass, species, and momenta balance laws applied to this material. We then examine the first and second thermodynamic laws and derive quantities and constraints for the model. Next, we model the Diels-Alder chemistry and thermal-chemical kinetics, which we subsequently use to model the rubbery shear modulus dependence on the extent of reaction as well as the rate and form of the network topology evolution (permanent shape change). Finally, we present the equilibrium and non-equilibrium Helmholtz free energy densities and calculate associated thermodynamic sensitivities.

Kinematics

We begin a discussion of kinetics and disclose the notation used throughout the rest of the text. Consider a homogenous body composed of a network polymer with reversible linkages which initially occupies the volume Ω_0 and has a boundary, $\partial\Omega_0$. This initial configuration is taken to be the time-independent reference configuration. The position of a material point within Ω_0 is denoted by, X_j, where we use Einstein's index notation. The motion of a material point from its position, X_j, in the reference configuration to its position, x_i, in the current configuration, wherein the body occupies the volume Ω with an associated boundary $\partial\Omega$, is assumed to be a smooth, bijective mapping, so that the inverse mapping always exists. The motion, displacement field u_i, material velocity, deformation gradient, and the volume ratio between the two configurations are,

$$x_i = \chi\left(X_i\right) = X_i + u_i, \qquad v_i = \dot{x}_i, \qquad F_{ij} = \frac{\partial x_i}{\partial X_j}, \qquad J = \det(F_{ij}) > 0. \tag{3.1}$$

Here, the overhead dot denotes the time derivative of a material point quantity. The notation used in this work distinguishes between reference and current configuration quantities via upper case and lower case letters respectively. For some quantities, however, the reference configuration is distinguished with an underscore $_0$. For example, the body in in the reference and current configuration occupies the volume Ω_0 and (Ω), respectively.

We take the polar decomposition of the deformation gradient to obtain the rotation, R_{ik}, and material stretch tensor, U_{kj}, and take the logarithm of the latter to generate the logarithmic (Hencky) strain, which is defined on the reference configuration.

$$F_{ij} = R_{ik} U_{kj}, \qquad \Upsilon_{ij} = \log(U_{ij}). \tag{3.2}$$

As is standard, we may additively split the Hencky strain into its spherical and deviatoric parts,

$$\Upsilon_{ij}^{sp} = \frac{\Upsilon_{kk}}{3} \delta_{ij}, \qquad \Upsilon_{ij}^{dev} = \Upsilon_{ij} - \Upsilon_{ij}^{sp}. \tag{3.3}$$

Here, we have employed the Kroenecker delta, δ_{ij}, to represent the identity tensor.

We use two invariants of the Hencky strain in the Helmholtz free energy function that are distinct from the standard Cayley-Hamilton invariants. Advantages of this choice have been discussed in other work relevant to polymer constitutive modeling [9]. We define the following two invariants of the Hencky strain tensor (using the properties of logarithms),

$$I_1[\Upsilon_{ij}] = \Upsilon_{ii} = \log(J) \tag{3.4}$$

$$I_2[\Upsilon_{ij}] = \Upsilon_{ij}\Upsilon_{ji} = \Upsilon_{ij}^{dev}\Upsilon_{ji}^{dev} + \frac{I_1[\Upsilon_{ij}]^2}{3}. \tag{3.5}$$

To separate invariant volumetric and deviatoric kinematics, we will use $I_1[\Upsilon_{ij}]$ and $I_2[\Upsilon_{ij}^{dev}] = I_2[\Upsilon_{ij}] - \frac{1}{3} I_1[\Upsilon_{ij}]^2$.

Mass, Species, and Momentum Balances

We briefly review the balance laws. The balance of mass at a material point relates the density in the current (ρ) and reference (ρ_0) configurations to the associated volume ratio (J),

$$\frac{\rho}{\rho_0} = J. \tag{3.6}$$

The chemical species must also satisfy individual conservation statements. Consider a particular species, labeled α, with number density defined in the reference configuration, N^α. The rate of change of the total number of species α within a subregion of the body, $\omega_0 \subset \Omega_0$ with the boundary $\partial \omega_0$, is denoted by $\dot{M}^{\alpha}_{\omega_0}$ and is given by,

$$\dot{M}^{\alpha}_{\omega_0} = \overline{\int_{\omega_0} N^{\alpha} dV}^{\,\cdot} = -\int_{\partial \omega_0} H^{\alpha}_i N_i dA + \int_{\omega_0} H^{\alpha} dV \tag{3.7}$$

Here, H^{α}_i, H^{α}, and N_i denote respectively the reference configuration species flux (number per area time), species source (number per volume), and unit normal vector associated with the differential reference area, dA. The overhead dot denotes a material time derivative, which commutes with the integral over the time-independent reference volume. Thus, with the divergence theorem, the local continuity equation for species α in the reference configuration is,

$$\dot{N}^{\alpha} = -\frac{\partial H^{\alpha}_i}{\partial X_i} + H^{\alpha} \tag{3.8}$$

We turn our attention to linear momentum and consider a quasi-static setting in which inertial effects are ignored. The local spatial balance of linear momentum at a material point is,

$$\frac{\partial \sigma_{ij}}{\partial x_i} + b_j = 0_j, \tag{3.9}$$

where σ_{ij} and b_j represent the Cauchy stress and body force vector defined per unit spatial volume. We assume an absence of micro polar moments, so that the angular momentum balance restricts the Cauchy stress to be symmetric ($\sigma_{ij} = \sigma_{ji}$). Later, we will find it useful to define material point quantities in the reference configuration, and so we introduce the symmetric Second Piola-Kirchoff stress, which is work conjugate to the material time derivative of the Green-Lagrange strain, as well as the First Piola-Kirchoff stress, which is work conjugate to the material time derivative of the deformation gradient,

$$S^{\Gamma}_{ij} = JF^{-1}_{ij}\sigma_{jk}F^{-1}_{lk}, \qquad \Gamma_{ik} = \frac{1}{2}(F_{ji}F_{jk} - \delta_{ik}), \qquad P_{ik} = J\sigma_{ij}F^{-1}_{kj}. \tag{3.10}$$

Here, Γ has been used so as not to confuse the Green-Lagrange strain and the total energy.

Energy Balance

We treat the body as a homogenous, single phase material that contains a total number of molecules of each chemical species $M^1, M^2, \ldots$. Neglecting kinetic energy, the time rate of change of the total energy in the body is composed of three quantities: the rate of mechanical work the body does against its surroundings ($\dot{W}_{out}$), the rate of chemical work that occurs as species change ($\dot{E}_{species}$), and the rate of thermal energy flowing into or generated within the body ($\dot{Q}_{in}$). The rate of total internal energy change in the body can then be written as,

$$\dot{E}_{total} = \dot{Q}_{total\ in} - \dot{W}_{by\ system} + \dot{E}_{species} \tag{3.11}$$

Here, we are considering a closed system and neglect species transport *across* the boundary of the body although thermal and mechanical energies can be exchanged between the body and its surroundings. From Eq. 3.11 and following Gurtin *et al.* 2010 or Chester and Anand 2011, we state the local form of the energy balance, with an internal energy density defined per unit reference volume, ε_0. Again, consider a subregion of the body in the reference configuration, denoted $\omega_0 \subset \Omega_0$, with its boundary $\partial\omega_0$. The rate of change of the total internal energy in this region is,

$$\begin{aligned}\dot{\overline{\int_{\omega_0} \varepsilon_0 dV}} &= -\int_{\partial\omega_0} Q_i N_i dA + \int_{\omega_0} Q dV \\ &\ldots + \int_{\partial\omega_0} P_{ij} N_j v_i dA + \int_{\omega_0} J b_i v_i dV \\ \ldots + \sum_{\alpha} \Bigg(&-\int_{\partial\omega_0} \mu^{\alpha} H_i^{\alpha} N_i dA + \int_{\omega_0} \mu^{\alpha} H^{\alpha} dV \Bigg).\end{aligned} \tag{3.12}$$

Here, Q_i and Q represent the referential thermal flux vector (energy per area time) and thermal source (energy per volume time). The energy associated with changing the referential number density of species α is characterized by the chemical potential, μ^{α} (energy per number of species). Employing the divergence theorem, the time-invariance of the reference configuration, the referential species conservation statements (Eq. 3.8), and the fact the size of the subregion can be made arbitrarily small, the local form of the energy balance is,

$$\dot{\varepsilon}_0 = -\frac{\partial Q_k}{\partial X_k} + Q + S^{\Gamma}_{ij}\dot{\Gamma}_{ij} + \sum_{\alpha}\left(\mu^{\alpha}\dot{N}^{\alpha} - H_i^{\alpha}\frac{\partial \mu^{\alpha}}{\partial X_i}\right), \tag{3.13}$$

wherein we have taken advantage of the fact that the internal stress power with respect to the First Piola-Kirchoff stress can also be written in terms of the Second Piola-Kirchoff stress and the Green-Lagrange strain, ($P_{ij}\dot{F}_{ij} = S^{\Gamma}_{ij}\dot{\Gamma}_{ij}$).

Entropy Production Inequality

We examine the Second Law of thermodynamics in the form of the Clausius-Duhem inequality within a referential subregion of the body,

$$\int_{\omega_0} \dot{\eta}_0 dV + \int_{\partial\omega_0} \frac{Q_i N_i}{\Theta} dA - \int_{\omega_0} \frac{Q}{\Theta} dV \geq 0, \tag{3.14}$$

wherein we define the referential entropy density, η_0, with units of energy per volume. Here we define the absolute temperature, Θ, which we require be greater than zero. The local form of Eq. 3.14 may be derived following similar arguments as above,

$$\dot{\eta}_0 - \frac{Q}{\Theta} + \frac{1}{\Theta}\frac{\partial Q_i}{\partial X_i} - \frac{Q_k}{\Theta^2}\frac{\partial \Theta}{\partial X_k} \geq 0 \tag{3.15}$$

By combining the local forms of the energy balance (Eq. 3.13) and the entropy production inequality (Eq. 3.15) through the elimination of heat source, Q, and multiplication of all terms by Θ, we arrive at,

$$\Theta\dot{\eta}_0 - \dot{\varepsilon}_0 + S^{\Gamma}_{ij}\dot{\Gamma}_{ij} - \frac{Q_k}{\Theta}\frac{\partial \Theta}{\partial X_k} + \sum_{\alpha}\left(\mu^{\alpha}\dot{N}^{\alpha} - H_i^{\alpha}\frac{\partial \mu^{\alpha}}{\partial X_i}\right) \geq 0 \tag{3.16}$$

The natural thermodynamic state variables for the internal energy density are the entropy, deformation gradient, and species number densities. It will be more convenient for us to represent the behavior of this system with a thermodynamic potential that uses temperature, rather than entropy, as a natural variable. Thus, the Helmholtz free energy density, defined per unit reference volume, is preferred and follows from the standard Legendre transform,

$$\Psi = \varepsilon_0 - \Theta\eta_0, \tag{3.17}$$

and upon taking the material time derivative of Eq. 3.17 and substituting the result into Eq. 3.16 and multiplying by (-1), we arrive at the principal inequality of rational mechanics (PIRM) [11],

$$\dot{\Psi} + \eta_0\dot{\Theta}_0 - S^{\Gamma}_{ij}\dot{\Gamma}_{ij} + \frac{Q_k}{\Theta}\frac{\partial \Theta}{\partial X_k} - \sum_{\alpha}\left(\mu^{\alpha}\dot{N}^{\alpha} - H_i^{\alpha}\frac{\partial \mu^{\alpha}}{\partial X_i}\right) \leq 0. \tag{3.18}$$

Eq. 3.18 is also known as the free energy imbalance (Gurtin *et al.* 2010), and it shows that the time evolution of thermodynamic state variables occurs in the direction that minimizes the free energy.

If we assume in general for reacting solid materials that the Helmholtz free energy is a function of Γ_{ij}, Θ, N^{α}, and $\{Z^1, Z^2, \ldots Z^n\}$, where Z^{β} are internal state variables that need not be thermodynamic state variables, then the material time derivative of the Helmholtz free energy density (per unit reference volume) is,

$$\dot{\Psi} = \frac{\partial \Psi}{\partial \Gamma_{ij}}\dot{\Gamma}_{ij} + \frac{\partial \Psi}{\partial \Theta}\dot{\Theta} + \sum_{\alpha}\left(\frac{\partial \Psi}{\partial N^{\alpha}}\dot{N}^{\alpha}\right) + \sum_{\beta}\left(\frac{\partial \Psi}{\partial Z^{\beta}}\dot{Z}^{\beta}\right). \tag{3.19}$$

Following the Coleman and Noll procedure in which we collect all terms directly related to rates of change of state variables and independently enforce that each one satisfies the PIRM (Eq. 3.18)

, we are restricted to define the stress, entropy, and chemical potential of each species as,

$$S^{\Gamma}_{ij} = \frac{\partial \Psi}{\partial \Gamma_{ij}}, \qquad \eta_0 = -\frac{\partial \Psi}{\partial \Theta}, \qquad \mu^{\alpha} = \frac{\partial \Psi}{\partial N^{\alpha}}. \tag{3.20}$$

It should be noted that the free energy descriptions in subsequent sections will depend on the first two invariants of the logarithmic strain tensor as defined by Eqs. 3.4 and 3.5, and thus, to recover the Second Piola-Kirchoff stress, the following transformation is needed [9],

$$S^{\Gamma}_{ij} = \frac{\partial \Psi}{\partial \Upsilon_{ab}} \frac{\partial \Upsilon_{ab}}{\partial \Gamma_{ij}} = S^{\Upsilon}_{ab} \frac{\partial \Upsilon_{ab}}{\partial \Gamma_{ij}}. \tag{3.21}$$

The transformation tensor between the logarithmic and the Green-Lagrange strains can be derived by considering differential changes to both principal stretches and directions but is not presented here for brevity. In Eq. 3.21, S^{Υ}_{ab} is the stress work conjugate to differential changes to the logarithmic strain, and so we call this quantity the Hencky stress. The remaining terms in the PIRM collectively represent a constraint on the rate of free energy dissipation (d^{diss}) as the Helmholtz free energy density evolves in time,

$$\mathrm{d}^{diss} = \sum_{\beta} \left(\frac{\partial \Psi}{\partial Z_{\beta}} \dot{Z}_{\beta} \right) + \sum_{\alpha} \left(H^{\alpha}_{i} \frac{\partial \mu^{\alpha}}{\partial X_i} \right) + \frac{Q_k}{\Theta} \frac{\partial \Theta}{\partial X_k} \leq 0, \tag{3.22}$$

In general, these thermodynamic and internal state variables may evolve independently. So, to guarantee that the entropy production inequality is satisfied for all possible changes to the system's thermodynamic state, we further restrict the time evolution of the Helmholtz free energy density, species fluxes, and thermal energy flux by requiring that each term in Eq. 3.22 satisfy the inequality separately,

$$\sum_{\beta} \left(\frac{\partial \Psi}{\partial Z_{\beta}} \dot{Z}_{\beta} \right) \leq 0, \qquad \sum_{\alpha} \left(H^{\alpha}_{i} \frac{\partial \mu^{\alpha}}{\partial X_i} \right) \leq 0, \qquad \frac{Q_k}{\Theta} \frac{\partial \Theta}{\partial X_k} \leq 0. \tag{3.23}$$

Equation of Motion for the Temperature Field

We define the specific heat capacity of the material at a constant state of deformation and relate it to the second order thermal sensitivity through the Legendre transform, Eq. 3.17, and Eq. 3.20,

$$C_F = \left(\frac{\partial \varepsilon_0}{\partial \Theta} \right)_{\Gamma_{ij}, N^{\alpha}, Z^{\beta}} = -\Theta \left(\frac{\partial^2 \Psi}{\partial \Theta \partial \Theta} \right)_{\Gamma_{ij}, N^{\alpha}, Z^{\beta}}. \tag{3.24}$$

As the entropy is given by the sensitivity of the Helmholtz free energy density with respect to temperature, Eq. 3.20, we may use the material time derivative of the Helmholtz free energy, Eq. 3.19, combined with the energy balance, Eq. 3.13, and the specific heat capacity, Eq. 3.24, to arrive at the equation of motion for the temperature field,

$$\begin{aligned} C_F\dot{\Theta} = Q - \frac{Q_i}{X_i} + \sum_{\alpha}\left(\Theta\frac{\partial^2\Psi}{\partial\Theta\partial N^{\alpha}}\dot{N}^{\alpha} - H_i^{\alpha}\frac{\partial\mu^{\alpha}}{\partial X_i}\right) \\ \ldots + \Theta\frac{\partial^2\Psi}{\partial\Theta\partial\Gamma_{ij}}\dot{\Gamma}_{ij} + \sum_{\beta}\left(\Theta\frac{\partial^2\Psi}{\partial\Theta\partial Z^{\beta}} - \frac{\partial\Psi}{\partial Z^{\beta}}\right)\dot{Z}^{\beta} \end{aligned} \tag{3.25}$$

Species and Thermal Energy Transport

Typically species and heat fluxes are constitutively specified to scale with the spatial gradients of the chemical potential and temperature respectively. We assume here that isotropic conditions occur so that in the current and reference configurations, the species and heat fluxes are constitutively specified as,

$$h_i^{\alpha} = -D^{\alpha}\frac{\partial\mu^{\alpha}}{\partial x_i}, \qquad q_i = -\kappa\frac{\partial\Theta}{\partial x_i}, \tag{3.26}$$

$$H_i^{\alpha} = -JD^{\alpha}F_{ij}^{-1}F_{kj}^{-1}\frac{\partial\mu^{\alpha}}{\partial X_k}, \qquad Q_i = -J\kappa F_{ij}^{-1}F_{kj}^{-1}\frac{\partial\Theta}{\partial X_k}. \tag{3.27}$$

Here, D^{α} and κ are the isotropic α-species and heat diffusion coefficients, defined in the current configuration and are material constants. With these constitutive rules, it is simple to show that the term-by-term requirements on the material's free energy dissipation rate are satisfied for the thermal and species diffusion terms, Eq. 3.23(2-3).

For the system considered in this work, we simplify our treatment by neglecting diffusion of the Diels-Alder species, A, F, and M so that $D^{\alpha} = 0$ for all α. This simplification is reasonable because chains that have been broken at F and M functionalities are still covalently tethered to the network. Thus, unless whole segments of chains are broken from the network, the individual species cannot diffuse long distances. Hence, we neglect diffusion of all of the chemical species. Under this simplification, the species number density conservation statements, Eq. 3.8, reduce to,

$$\dot{N}^{\alpha} = H^{\alpha}. \tag{3.28}$$

Therefore, the time evolution of species densities are related only to source terms, and so these conservation statements reduce a system of ordinary differential equations at each material point rather than partial differential equations across the body (when diffusion occurs).

Diels-Alder Chemistry

We now describe the chemical reaction involved in this system as the species densities, and their associated chemical potentials, will directly enter into the free energy density that we develop. As discussed in section 1, we are considering a thermally reversible chemical reaction of the form,

$$F + M \leftrightarrow A \tag{3.29}$$

This reaction is responsible for connecting chains (forward reaction) or breaking them apart (reverse reaction), and so, the number density of chains and shear modulus will scale with the extent to which the reaction is in the bonded (forward) state. The total species referential number density, which should not be confused with the reference configuration surface normal vector, is,

$$N = N^A + N^F + N^M \tag{3.30}$$

The total number density, N, in Eq. 3.30 is not a conserved quantity, but assuming that Eq. 3.29 is the only chemical reaction occurring in the system and that there is no species diffusion (see section 3), there is a conserved species density, which represents the maximum referential density that any species can obtain, which is defined as,

$$\phi = N^A + \frac{1}{2}\left(N^F + N^M\right). \tag{3.31}$$

With ϕ, we can define the extent of the chemical reaction,

$$N^A = \phi x, \qquad x \in [0,1]. \tag{3.32}$$

In the experimental system from the literature that will be modeled in this work, the polymer network is formulated with an equal mol fraction of furan and maleimide species, and since they bond in a 1:1 ratio (from Eq. 3.29), the number densities of furan and maleimide species are the same in this work. Therefore, we may write the number densities in terms of the extent of reaction and the total conserved species density, ϕ:

$$N^F = N^M = \phi(1-x), \qquad N = \phi(2-x). \tag{3.33}$$

For the experimental system considered in this work, Bowman and co-workers measured the equilibrium extent of reaction as a function of temperature in a state of constant stress. Specifically, the specimens in their studies were not subjected to any applied mechanical stresses other than ambient pressure. Under such conditions, the Gibbs free energy of the system is the natural thermodynamic potential with which to consider the equilibrium conditions for the reaction. We define the reaction equilibrium constant following the stoichiometric relationship of the chemical reaction (Eq. 3.29),

$$K^{\infty}[\Theta] = \frac{N^A_{\infty}/\phi}{(N^F_{\infty}/\phi)(N^M_{\infty}/\phi)} = \frac{x}{(1-x)^2}, \tag{3.34}$$

wherein "∞" indicates that the quantities have equilibrated at the temperature, Θ, and do not change in time. Note that this definition is dimensionless compared to the one used by Bowman and co-workers, which defines the equilibrium constant as the ratio of species densities and thus has units. By empirically examining the temperature dependence of $K^{\infty}[\Theta]$ in Eq. 3.34, Bowman and co-workers calculated the standard enthalpy and entropy of the reaction via the Van't Hoff equation,

$$\log K^{\infty} = -\frac{\Delta g^{\circ}_{rxn}}{RT} = -\frac{-\Delta H^{\circ}_{rxn}}{R\Theta} + \frac{\Delta \eta^{\circ}_{rxn}}{R}, \tag{3.35}$$

wherein R denotes the universal gas constant, and Δg°_{rxn}, ΔH°_{rxn}, and $\Delta \eta^{\circ}_{rxn}$ denote the standard changes in Gibbs free energy, enthalpy, and entropy due to the reaction. These quantities determine the associated quantity change that is accompanied when one mol of the products (species A) is formed from the reactants (species F and M) under standard conditions (typically 1 atm pressure and at 25 Celsius).

Under a constant state of stress and at a constant temperature, the equilibrium condition for the material is that the Gibbs free energy is at a minimum so that its total differential is zero,

$$\begin{aligned} 0 = dg|_{\Theta, S^{\Upsilon}_{ij}} = \Upsilon_{ij} dS^{\Upsilon}_{ij} - \eta_0 d\Theta + \sum_{\alpha=A,F,M} (\mu^{\alpha} dN^{\alpha} + d\mu^{\alpha} N^{\alpha}) \\ \ldots = \sum_{\alpha=A,F,M} (\mu^{\alpha} dN^{\alpha}), \end{aligned} \tag{3.36}$$

where we have used the fact that under the equilibrium conditions considered here, $dS^{\Upsilon}_{ij} = 0_{ij}$, $d\Theta = 0$, and the Gibbs-Duhem equality,

$$\sum_{\alpha=A,F,M} (d\mu^{\alpha} N^{\alpha}) = -\Upsilon_{ij} dS^{\Upsilon}_{ij} + \eta_0 d\Theta = 0. \tag{3.37}$$

Equation 3.37 gives the expected statement of chemical equilibrium at a fixed temperature and stress. To produce the temperature-dependent equilibrium constant, Eqs. 3.34 and 3.35, we model the chemical potentials for each species as,

$$\mu^A = \mu^{A\circ} + R\Theta \log(a_A), \qquad a_A = \frac{N^A}{N}, \tag{3.38}$$

$$\mu^F = \mu^{F\circ} + R\Theta \log(a_F), \qquad a_F = \frac{N^F}{N}, \tag{3.39}$$

$$\mu^M = \mu^{M\circ} + R\Theta \log(a_M), \qquad a_M = \frac{N^M}{N}. \tag{3.40}$$

Here, a_α represents the ideal activity of species α. Non-ideal behavior is captured by the temperature dependent standard chemical potentials of each species, $\mu^{\alpha\circ}$. From the condition of equilibrium at a constant pressure and temperature, Eq. 3.37, the equilibrium constant relationships (Eqs. 3.34 and 3.35), and the chemical potentials, it can be shown that the Gibbs-Duhem equality is satisfied (Eq. 3.37) and that,

$$\mu^{A\circ} - \mu^{F\circ} - \mu^{M\circ} = \Delta g^{\circ}_{rxn}. \tag{3.41}$$

Using the extent of reaction variable, x, a single chemical potential may be used to characterize the thermodynamic force associated with changes to the chemical state of the system,

$$\mu^{(x)} = \frac{\partial g}{\partial x}. \tag{3.42}$$

The condition of chemical equilibrium with respect to the extent of reaction is $\mu^{(x)} = 0$, which reproduces the previous statement of chemical equalibrium, Eq. 3.41. However, via Eq. 3.42, we have a convenient way to include the effects on chemical equilibrium of coupling terms in the free energy. That is, we may include couplings between the extent of reaction, x, the absolute temperature, Θ, and the first and second invariants of the logarithmic strain, $I_1[\Upsilon]$ and $I_2[\Upsilon]$ respectively. If such terms are included, then the condition of chemical equilibrium will differ from Eqs. 3.41 and 3.42.

Diels-Alder Reaction Kinetics

Our objective here is to determine the rates of the forward and reverse Diels-Alder reactions (Eq. 3.29), which is related to the rates at which the number density of network chains is increasing and decreasing. The forward and reverse reactions determine the source terms in the species balance laws, Eq. 3.8, and so without diffusion, the reaction kinetics determine the rates of change of the species densities directly; see Eq. 3.28. Recall that an equal stoichiometry of furan and malemide was used in the system under examination (see Eq. 3.33). Following Bowman and coworkers, we model that the Diels-Alder reaction kinetics via a second-order thermally activated model so that the referential species densities along with the conservation requirement, Eq. 3.31, obey in the following kinetics,

$$\dot{N}^F = \dot{N}^M = -k^f N^F N^M + k^r N^A, \qquad \dot{N}^A = k^f N^F N^M - k^r N^A. \tag{3.43}$$

These kinetics are a manifestation of the law of mass action, which is reasonable here since we expect that the Diels-Alder reaction occurs as a single step reaction. Here, k^f and k^r are the temperature dependent forward and reverse reaction rate constants. The first term in Eq. 3.43(1) represents the rate at which the number density of chains is increasing due to the forward reaction while the second term gives the rate of decrease of the number density of chains associated with the reverse reaction. We may relate the reverse and forward reaction rates to the rate of change of the extent of reaction from Eqs. 3.32, 3.33, and 3.43,

$$\dot{x}^{-} = k^{r}\phi x, \qquad \dot{x}^{+} = k^{f}\phi(1-x)^{2}, \qquad \dot{x} = \dot{x}^{+} - \dot{x}^{-}. \tag{3.44}$$

At equilibrium, the species evolutions are zero, so that the forward and reverse rate constants are related to the equilibrium constant via,

$$\frac{k^{f}}{k^{r}} = \frac{K^{\infty}[\Theta]}{\phi}. \tag{3.45}$$

Bowman and co-workers assumed that these rate constants are thermally activated, so that, along with Eq. 3.45, they are specified as,

$$k^{r} = k^{0}\exp\left[\frac{-E_{act}}{R\Theta}\right], \tag{3.46}$$

where the prefactor, k^0, and activation energy, E_{act}, are determined experimentally. However, these reaction kinetics do not account for the arresting effects of vitrification. Thus, we assume that the thermally activated rate acts in parallel with the material (viscous) time scale of the network following previous work [3, 22, 1],

$$k^{r} = k^{visco}k^{0}\exp\left[\frac{-E_{act}}{R\Theta}\right] = \frac{k^{0}}{a_{mat}}\exp\left[\frac{-E_{act}}{R\Theta}\right]. \tag{3.47}$$

Consequently, if the material time scale becomes very long, as it does in when the network is in the glassy state, then the reaction rate is arrested.

Shear Modulus Dependence on the Chemical Species

In the flexible chain limit of rubber elasticity, the shear modulus of the network depends linearly on the number density of chains beyond the gel-point extent of reaction as well as linearly on the absolute temperature. Following this insight, we model the equilibrium shear modulus via,

$$G^{\infty}[\Theta,x] = \frac{G^{\infty}_{ref}\Theta\left(x-x_{gel}\right)}{\Theta_{ref}\left(x_{ref}-x_{gel}\right)} = \bar{G}\Theta\left(x-x_{gel}\right), \tag{3.48}$$

which allows us to calibrate the shear modulus the experimentally measured value at a reference temperature, G^{∞}_{ref}. Note that $\bar{G}$ lumps the reference property material constants into one variable for convenience. The gel point extent of reaction, x_{gel}, is a fundamental geometric/topological property of the network and does not depend on temperature, state of stress, etc.

Under conditions of chemical equilibrium, the rubbery shear modulus in Eq. 3.48 depends non-linearly on temperature since the extent of reaction depends exponentially on temperature. Hence, this shear modulus representation may vary substantially more over a given temperature range than a traditional thermoset. Mechanistically, this model feature is sensible since in thermosets with thermally reversible functionalities, the number density of chains changes is not constant.

However, in the short chain limit, the shear modulus of the network scales non-linearly with the number density of chains. For example, for epoxy networks cured via a step-growth reaction with di-functional epoxy monomers, Adolf and Chambers [3] report that the shear modulus scales with the curing extent of reaction via,

$$G[y] = G[1]\left(\frac{(y^2 - y_{gel}^2)^{2.7}}{1 - y_{gel}^2}\right). \tag{3.49}$$

Here, y_{gel} is the curing extent of reaction when the network has reached the percolation limit (gel point). The temperature dependence is not included in Eq. 3.49, and it need not be linear in temperature. For simplicity, we adopt the ideal shear modulus and temperature dependence scaling of Eq. 3.48 and recognize that this choice may be a substantial oversimplification.

Using the reaction kinetics written in terms of the reaction extent, Eq. 3.44 and the shear modulus dependence on the adduct species density, Eq. 3.48, the material time derivate of the shear modulus takes the following form,

$$\dot{G}^\infty = \bar{G}\dot{\Theta}\left(x - x_{gel}\right) + \bar{G}\Theta\dot{x} = \bar{G}\dot{\Theta}\left(x - x_{gel}\right) + \dot{G}_+^\infty - \dot{G}_-^\infty, \tag{3.50}$$

$$\dot{G}_-^\infty = \bar{G}\Theta\phi k^r x, \qquad \dot{G}_+^\infty = \bar{G}\Theta\phi k^f (1-x)^2. \tag{3.51}$$

Here, $\dot{G}_+^\infty$ and $\dot{G}_-^\infty$ denote the rates of increase and decrease of the shear modulus due to the addition and destruction of the referential number density of chains.

Evolution of the Stress-Free Configuration

Next, we discuss the effects of network topology evolution on the stress-free shape of the body, which provides the network a mechanism to take on a new permanent shape. Phenomenologically, we capture this behavior through the time evolution of the stress-free strain tensor internal state variable following the polymer curing work of Adolf and Chambers [3]. We note that considerable theoretical and computational efforts have explored the concept of stress-free configurations as a means of explaining compression set in elastomers. Tobolsky proposed the Two-Network Hypothesis [8], examined theoretically by Flory [12], and computationally by Rottach and co-worker

[28]. This approach has been applied with success to a variety of problems associated with the continuum thermomechanical behavior of temperature sensitive elastomers [31, 35] and photo-mechanically coupled polymers [18]. The Two-Network approach is based on a multiplicative decomposition of the deformation gradient,

$$F_{ij}^{total} = F_{ik}^{2} F_{kj}^{1}, \tag{3.52}$$

such that the elastic free energy of the first and second network volume fractions depend on F_{ij}^{total} and F_{ik}^{2} respectively. For example, often in the literature, the total elastic free energy of a two-network material is,

$$\Psi_{elasticF_2F_1} = v_1 \Psi(F_{ik}^{2} F_{kj}^{1}) + v_2 \Psi(F_{ij}^{2}) \tag{3.53}$$

There are two issues with this multiplicative split. First, the stress-free configuration of the material depends on the specific constitutive functions involved ($\Psi(\bullet)$), and second, if the intermediate configuration F_{kj}^{1} is evolved, for example through the evolution of the network topology, then the minimum free energy shape evolves in a complicated manner that is strongly dependent on the constitutive function as well. Some work has looked into evolving the intermediate configuration for polymers experiencing microstructural evolution [13, 19, 27], but we choose a more intuitive approach.

As mentioned above, we model the effect of an evolving network topology by directly evolving a stress-free strain tensor, ξ_{ij}, subject to the following assumptions,

- Volumetric deformation, which is dominated by Van-der-Waals interactions in polymer networks, does not induce a change in the stress free configuration.
- Deviatoric deformation moves chains past each other, so that as chains break and reform, they may do so in different configurations. An aggregate number of such events reduces the elastic free energy.
- The stress-free configuration may only evolve if it is different from the current state of deformation, $\Upsilon_{ij}^{dev} - \xi_{ij}^{dev} \neq 0_{ij}$
- The rate of change of the stress-free configuration scales with the rate of increase of the equilibrium shear modulus due to the *formation* of chains, $\dot{G}^{+}$ in Eq. 3.51.
- The rate of decrease of the equilibrium shear modulus due to chain scission does not affect the stress-free configuration.

Following Adolf and Chambers (2007) and these hypothesis, we model the material time derivative of the stress free strain tensor is,

$$\dot{\xi}_{ij} = \frac{G^{+}}{G^{\infty}} \left(\Upsilon_{ij}^{dev} - \xi_{ij}^{dev} \right). \tag{3.54}$$

One important inadequacy of this rule is that it does not account for the change of the stress-free configuration due to chain scission (assumption 4), which, as pointed out in many theoretical investigations, involves a load transfer from chains as they are scissioned to the surrounding network [28, 12]. However, these theoretical treatments consider the special case of just 2 states of strain. Here, we are concerned with an arbitrary number of strained configurations, and so in this work, we neglect the influence of scissioned chains on the evolution of the stress free configuration.

Additive Split of the Helmholtz Free Energy Density

From the experimental observations in section 2, we develop a Helmholtz free energy density, consistent with the PIRM (Eq. 3.18), to describe the thermal-chemical-mechanical behavior of network polymers with reversible linkages. We assume that the Helmholtz free energy, per unit reference volume, is a function of the following state variables:

Υ_{ij} The logarithmic strain tensor.

Θ The absolute temperature.

N^{α} The referential number density of each chemical species, $\alpha = A,F,M$. These number densities are related to the extent of reaction definition, Eq. 3.32, and they obey their own conservation statements, Eq. 3.8.

ξ_{ij} The stress-free strain tensor, which represents the evolving permanent shape of thematerial point due to the topological rearrangement of the network.

We model the material's referential Helmholtz free energy in two parts,

$$\Psi\left(\Upsilon_{ij},\Theta,N^{\alpha},\xi_{ij}\right) = \Psi^{\infty} + \Psi^{visco}. \tag{3.55}$$

The first component, Ψ^{∞}, represents the equilibrium network response with respect to changes to the thermodynamic state. For example, from it, the rate independent heat capacity, stress, or chemical state can be derived. However, if the network topology is changing, the equilibrium free energy will decay in time as stress is relaxed in the network. The second term, Ψ^{visco}, represents a non-equilibrium free energy penalty that the material suffers when the thermodynamic state is changed too quickly relatively to its own internal time scale. Classically, this free energy penalty gives rise to altered stresses, heat capacities, and thermal expansion behaviors that distinguish the polymer's non-equilibrium glassy state compared with its equilibrium rubbery state.

The additive split of the free energy density into equilibrium and non-equilibrium parts (Eq. 3.55), results in an additive split of each of the generalized thermodynamic forces into equilibrium and non-equilibrium parts. Thus, from Eqs. 3.55 and 3.23 the Second Piola-Kirchoff stress, the entropy, and the chemical potential of each species also split into equilibrium and non-equilibrium contributions,

$$S^{\Gamma}_{ij} = S^{\Gamma\infty}_{ij} + S^{\Gamma visco}_{ij}, \qquad \eta_0 = \eta_0^{\infty} + \eta_0^{visco}, \qquad \mu^{\alpha} = \mu^{\alpha\infty} + \mu^{\alpha visco}. \tag{3.56}$$

Analogously, the thermodynamic work conjugate fluxes associated with the internal state variables (Z_β) also may be split into equilibrium and non-equilibrium parts.

Equilibrium Free Energy Contributions

We first examine the equilibrium referential Helmholtz free energy density, which we further divide into four parts arising from elastic, thermal, chemical, and mixed free energy contributions:

$$\Psi^{\infty}\left(\Upsilon_{ij}, \Theta, N^{\alpha}, \xi_{ij}\right) = \Psi^{\infty}_{elastic} + \Psi^{\infty}_{thermal} + \Psi^{\infty}_{chemical} + \Psi^{\infty}_{mixed} + \Psi_{ref}, \tag{3.57}$$

$$\Psi^{\infty}_{elastic} = P_{ref} I_1[\Upsilon] + \frac{K^{\infty}}{2}(I_1[\Upsilon])^2 + G[x,\Theta]\, I_2\left[\Upsilon^{dev}_{ij} - \xi^{dev}_{ij}\right], \tag{3.58}$$

$$\Psi^{\infty}_{thermal} = \frac{C_{F0}}{\rho_{ref}}\left(\Theta - \Theta_{ref} - \Theta \log\left(\frac{\Theta}{\Theta_{ref}}\right)\right) - \frac{C_{F1}}{2\rho_{ref}\Theta_{ref}}(\Theta - \Theta_{ref})^2, \tag{3.59}$$

$$\Psi^{\infty}_{chemical} = \sum_{\alpha}\left(\mu^{\alpha} N^{\alpha}\right), \tag{3.60}$$

$$\Psi^{\infty}_{mixed} = -K^{\infty}\beta^{\infty}(x - x_{ref}) I_1[\Upsilon] - K\alpha^{\infty}(\Theta - \Theta_{ref}) I_1[\Upsilon]. \tag{3.61}$$

Throughout these equations, a reference state is referred to which characterizes the initial free energy density. The extent of the chemical reaction, x, is also used for convenience and is related to the referential species densities through Eq. 3.32. The chemical potential, associated with each species, is modeled via Eq. 3.38, 3.39, and 3.40. We summarize the material properties in table 3.

It is important to note that a simple form of the elastic free energy density is used. For other systems, another constitutive equation for the elastic free energy may be more appropriate. Also, note that the shear modulus, $G[x,\Theta]$, is assumed to be a function of the extent of reaction as well as the absolute temperature as discussed in section 3. There are several additional assumptions built into the equilibrium free energy density that will be discussed in subsequent sections.

Following, Eqs. 3.20 and 3.21, we derive the equilibrium contribution to S^{Υ}_{ij},

$$S^{\Upsilon\infty}_{ij} = \frac{\partial \Psi^{\infty}}{\partial \Upsilon_{ij}} = 2G[x,\Theta](\Upsilon^{dev}_{ij} - \xi^{dev}_{ij}) \tag{3.62}$$
$$\ldots + \left(P_{ref} + K^{\infty} I_1[\Upsilon] - K^{\infty}\beta^{\infty}(x - x_{ref}) - K^{\infty}\alpha^{\infty}(\Theta - \Theta_{ref})\right)\delta_{ij}.$$

We also calculate the referential entropy density and chemical potential with respect to a change in the extent of reaction variable, x, from Eqs. 3.20 and 3.42,

$$\eta_0 = \frac{C_{F0}}{\rho_{ref}} \log\left(\frac{\Theta}{\Theta_{ref}}\right) + \frac{C_{F1}}{\rho_{ref}\Theta_{ref}}(\Theta - \Theta_{ref}) \tag{3.63}$$

$$\ldots - \frac{\partial G[x,\Theta]}{\partial \Theta} I_2\left[\Upsilon_{ij}^{dev} - \xi_{ij}^{dev}\right] + K^{\infty}\alpha^{\infty} I_1\left[\Upsilon_{kk}\right],$$

$$\mu^{(x)} = \phi\left(\mu^{(A)} - \mu^{(F)} - \mu^{(M)}\right) - K^{\infty}\beta^{\infty} I_1[\Upsilon_{kk}] + \frac{\partial G[x,\Theta]}{\partial x} I_2\left[\Upsilon_{ij}^{dev} - \xi_{ij}^{dev}\right]. \tag{3.64}$$

Two interesting results emerge from the choice of the equilibrium Helmholtz free energy. First, the referential entropy density depends on the volumetric state of deformation and shear modulus sensitivity with respect to temperature. However, these dependences do not influence the specific heat capacity at constant deformation from Eq. 3.24(2) given the linear sensitivity of the shear modulus with respect to temperature from Eq. 3.48. Second, the condition of chemical equilibrium with respect to the extent of reaction, that $\mu^{(x)} = 0$, now includes dependencies on the volumetric deformation (I_1), shear deformation (I_2), and the shear modulus sensitivity with respect to x. Even under isothermal conditions, chemical equilibrium can be changed if the material is subjected to substantial deformation.

Non-Equilibrium Helmholtz Free Energy Contributions

Next, we develop the non-equilibrium free energy penalties that the system experiences when its thermodynamic state is changed faster than its characteristic time scale. Here we adopt the simplified potential energy clock model (SPEC) developed by Adolf and co-workers [5]. We only summarize the pertinent results needed to represent the viscous behavior of polymers with removable linkages. We assume that the non-equilibrium contributions are sufficiently small that we may approximate them with functional Taylor expansions about the equilibrium state. We consider viscoelastic dependencies related to the time histories of the logarithmic strain different from the stress-free strain tensor (ξ_{ij}), the absolute temperature, and the extent of reaction each to second-order along with certain combinations of cross-terms. Distinctively missing are cross-terms that couple the shear deformation history with the extent of reaction as well as with the temperature history. As discussed in section, 3, we have neglected the coupling between the network topology and volumetric responses. The non-equilibrium free energy penalty taken from the SPEC model is,

$$\begin{aligned}
\Psi^{visco} &= \frac{1}{2}(K^{G}-K^{\infty})\int_{0}^{t}ds\int_{0}^{t}duf^{1}\left(t'-s',t'-u'\right)\frac{dI_{1\Upsilon}}{ds}\frac{dI_{1\Upsilon}}{du} \\
&+\frac{1}{2}(G^{G}-G^{\infty})\int_{0}^{t}ds\int_{0}^{t}duf^{2}\left(t'-s',t'-u'\right)\frac{d(\Upsilon_{ij}^{dev}-\xi_{ij}^{dev})}{ds}\frac{d(\Upsilon_{ij}^{dev}-\xi_{ij}^{dev})}{du} \\
&+\frac{1}{2}\frac{(C_{FG}-C_{F\infty})}{\Theta_{ref}}\int_{0}^{t}ds\int_{0}^{t}duf^{5}\left(t'-s',t'-u'\right)\frac{d\Theta}{ds}\frac{d\Theta}{du} \\
&-(K^{G}\alpha^{G}-K^{\infty}\alpha^{\infty})\int_{0}^{t}ds\int_{0}^{t}duf^{3}\left(t'-s',t'-u'\right)\frac{dI_{1\Upsilon}}{ds}\frac{d\Theta}{du} \\
&-(K^{G}\beta^{G}-K^{\infty}\beta^{\infty})\int_{0}^{t}ds\int_{0}^{t}duf^{4}\left(t'-s',t'-u'\right)\frac{dI_{1\Upsilon}}{ds}\frac{dx}{du} \\
&+(\eta_{rxnG}-\eta_{rxn\infty})\int_{0}^{t}ds\int_{0}^{t}duf^{6}\left(t'-s',t'-u'\right)\frac{d\Theta}{ds}\frac{dx}{du}
\end{aligned} \tag{3.65}$$

The functions, $\{f^{k}\}$, are different relaxation functions, expanded here as Proney series,

$$f^{k}\left(t'-s',t'-u'\right)=\sum_{j=1}^{m}A^{j}\exp\left(\frac{-\left(t'-s'\right)}{\tau_{j}}\right)\exp\left(\frac{-\left(t'-u'\right)}{\tau_{j}}\right) \tag{3.66}$$

The Proney Series satisfy a normalization condition that $f^{k}(0,0)=\sum_{j=1}^{m}A^{j}=1$, and the arguments, $t'-s'$ and $t'-u'$ represent the difference in material time between t' and s'. The material time is related to the laboratory time scale, t, through the viscoleastic shift factor, a, such that $t'=\frac{t}{a}$. The viscoelastic shift factor is an internal state variable which is itself a function of the deformation, temperature, and reaction histories. The component pairs, (τ_{j}, A^{j}), represent individual relaxation times and weights associated with the relaxation spectrum f^{k}. Typically, these experimentally determined relaxation spectra are first represented through stretched exponentials which are later fit with a least-squared projection onto the Proney basis in Eq. 3.66. For example, the volumetric and shear relaxation spectra at the viscoelastic reference temperature, which may be chosen to be the glass transition temperature, are characterized by two parameters each (τ_{v},γ_{v}) and (τ_{s},γ_{s}) through,

$$f^{v}(t)=\exp\left(\left(\frac{-t}{\tau_{v}}\right)^{\gamma_{v}}\right),\quad f^{s}(t)=\exp\left(\left(\frac{-t}{\tau_{s}}\right)^{\gamma_{s}}\right). \tag{3.67}$$

Here, (τ_{k},γ_{k}) and (τ_{m},γ_{m}) are material constants and no sum is applied on these subscripsts.

To simplify matters, we assume that all relaxation spectra obey a common time-temperature superposition, which is the statement rheological simplicity. This assumption may be invalid if the material is transitioned across its gel-point and becomes a liquid. As an example, for a rheologically simple material, the complex shear modulus as measured from dynamic mechanical analysis obeys the following relationship,

$$G^*(\omega,\Theta) = G^*(a_\Theta \omega, \Theta_{ref}) \tag{3.68}$$

Following the SPEC model, we use the phenomenological representation of the viscoelastic shift factor's dependence on the temperature, shear, and volumetric deformation histories,

$$\log a = \frac{-C_1 N}{C_2 + N}, \tag{3.69}$$

$$\begin{aligned} N = &\left(\Theta - \Theta_{glass} - \int_0^t ds f_3\left(t'-s',0\right)\frac{dT}{ds}\right)\dots \\ &+C_3\left(I_1[\Upsilon] - \int_0^t ds f_1\left(t'-s',0\right)\frac{dI_{1\mathbf{H}}}{ds}\right)\dots \\ &+C_4\int_0^t ds\int_0^t du f^2\left(t'-s',t'-u'\right)\frac{d(\Upsilon_{ij}^{dev}-\xi_{ij}^{dev})}{ds}\frac{d(\Upsilon_{ij}^{dev}-\xi_{ij}^{dev})}{du}. \end{aligned} \tag{3.70}$$

Here, C_{1-4} are material constants the determine the sensitivity of the viscoelastic time scale with respect to temperature change (C_1, C_2), volumetric deformation (C_3), and shear deformation (C_4). The material time scale can then be calculated as a function of the thermal, volumetric and shear deformation histories through,

$$t'-s' = \int_s^t \frac{dz}{a(z)}dz. \tag{3.71}$$

From the equilibrium and non-equilibrium Helmholtz Free energy densities in Eqs. 3.57 and 3.65, the Hencky Stress is derived, with the equilibrium term denoted by $S_{ij}^{\Upsilon\infty}$, given by Eq. 3.62.

$$\begin{aligned} S_{ij}^{\Upsilon} = \frac{\partial\Psi}{\partial\Upsilon_{ij}} = S_{ij}^{\Upsilon\infty} &+ (K^G - K^\infty)\int_0^t ds f_1\left(t'-s',0\right)\frac{dI_1[\Upsilon]}{ds}\delta_{ij} \\ &+(G^G - G^\infty)\int_0^t ds f_2\left(t'-s',0\right)\frac{d(\Upsilon_{ij}^{dev}-\xi_{dev})}{ds} \\ &-(K^G\alpha^G - K^\infty\alpha^\infty)\int_0^t ds f_3\left(t'-s',0\right)\frac{dT}{ds}\delta_{ij} \\ &-(K^G\beta^G - K^\infty\beta^\infty)\int_0^t ds f_4\left(t'-s',0\right)\frac{dx}{ds}\delta_{ij} \end{aligned} \tag{3.72}$$

The non-equilibrium constants, ψ_i, can be related to standard thermodynamic quantities, so that the total Helmholtz free energy, entropy, and Hencky stress are given by,

$$\eta = -\left(\frac{\partial\Psi}{\partial T}\right)_{\Upsilon,x,\xi}, \tag{3.73}$$

$$
\begin{aligned}
&= \eta_{ref} + \frac{C_{V\infty}}{T_{ref}} \left(T - T_{ref}\right) + \eta_{rxn} \left(x - x_{ref}\right) - K^{\infty} \alpha_{\infty} I_{\Upsilon} \\
&\quad -(K^{G}\alpha^{G} - K^{\infty}\alpha^{\infty}) \int_0^t ds f_3 \left(t' - s', 0\right) \frac{dI_1[\Upsilon]}{ds} \\
&\quad \frac{(C_{VG} - C_{V\infty})}{T_{ref}} \int_0^t ds f_5 \left(t' - s', 0\right) \frac{dT}{ds} \\
&\quad +(\eta_{rxnG} - \eta_{rxn\infty}) \int_0^t du f_6 \left(t' - s', 0\right) \frac{dx}{du}.
\end{aligned}
$$

Model Parameters and Experiments Necessary to Populate Them

The removable polymer model involves three categories of parameters. The first set contains the thermal-chemical equilibrium and kinetics constants associated with the Diels-Alder chemistry, which is summarized in table 3.1. The second and third sets are respectively associated with the rubbery and glassy thermal-mechanical properties and are summarized in tables 3 and 3.3.

Bowman and co-workers discuss using FTIR to measure the temperature dependence of the equilibrium constant as well as to determine the thermally activated parameters associated with the forward and reverse reactions [6], and supplementary material for this reference describes the process of fitting the Arrhenius kinetics parameters. However, they did not measure the volume change as a function of the extent of reaction, and likely assumed that it is negligible particularly in the gelled state of the material. Still, other systems could involve a volume change with extent of reaction, which would be difficult to deconvolve from thermal expansion. Likely the best method is simply to use a Thermal Mechanical Analyzer, and lump both volume changes due to temperature and change in equilibrium extent of reaction into a non-linear, temperature dependent thermal expansion coefficient. One other property related to the structure of the polymer network and the reversible chemistry is the gel point extent of reaction, which can be determined as the extent of reaction corresponding to the temperature at which the storage and loss-moduli have similar frequency scalings, which is known as the Winter-Cambrion criterion [36]. This property can therefore be determined from isothermal frequency sweep DMA data.

Mechanical properties associated with the equilibrium Helmholtz free energy density (Eq. 3.57) are summarized in 3. For the RPM model, two isotropic (and isothermal) linear elastic constants are needed, which could be derived from storage shear and compression (or tensile) moduli in DMA. Thermal properties involve measurements of the thermal conductivity and the enthalpy (from which the specific heat capacity at constant pressure can be derived).

The final set of properties are associated with the glassy behavior. A detailed discussion of this topic can be found in reference [4], and the interested reader is directed there. However, there is one additional subtlety compared with traditional thermosets. For RPM materials, relaxation behavior of different thermodynamic properties at different temperatures near the glass transition may be difficult to acquire without pollution from the relaxation behavior of the polymer network due to the reversible chemistry. This scenario would occur if the glass transition is relatively high (close to the gel point temperature) as the chemical kinetics would be fast. If the glass transition is far below the gel point temperature, than this issue is likely minimal. A summary of system parameters is supplied below.

Parameter	**Units**	**Description**
Θ_{ref}	K	Initial temperature
x_{ref}	none	Initial extent of reaction
x_{gel}		Gel-point extent of reaction
D^{α}	m^2 s $^{-1}$	Isotropic spatial diffusivity of species α
κ	J m^{-1} K^{-1} s^{-1}	Isotropic, spatial thermal conductivity
β^{∞}	none	Equilibrium volumetric deformation associated with the chemical reaction extent
ϕ	mol m^{-3}	The maximum concentration (per unit reference volume) that any species can obtain.
ΔH°_{rxn}	J	Standard enthalpy change associated with the Diels-Alder reaction
$\Delta \eta^{\circ}_{rxn}$	J K^{-1}	Standard entropy change associated with the Diels-Alder reaction
k_0	s^{-1}	Prefactor to the Arrhenius chemical kinetics.
E_{act}	J	Activation energy associated with the Arrhenius reaction kinetics.

Table 3.1. Properties of the Diels-Alder chemistry and transport

Parameter	**Units**	**Description**
P_{ref}	Pa	First Piola-Kirchoff pressure datum (ambient pressure)
K^{∞}	Pa	Equilibrium bulk modulus
G^{∞}_{ref}	Pa	Equilibrium shear modulus at the reference temperature, Θ_{ref}
C_{F0}	J kg^{-1} K^{-1}	Specific heat capacity at a fixed state of deformation. This constant weights a term that produces a constant response with respect to temperature.
C_{F1}	J kg^{-1} K^{-1}	Specific heat capacity at a fixed state of deformation. This constant weights a term that produces a linear response with respect to temperature.
α_{∞}	K^{-1}	Equilibrium volumetric thermal expansion coefficient

Table 3.2. Equilibrium helmholtz free energy density parameters.

Parameter	Units	Description
Θ_{glass}	K	Nominal glass transition temperature
Ψ_{ref}	Pa	Helmholtz free energy density datum in the initial state of the material point
K^G	Pa	Glassy bulk modulus
G_G	Pa	Non-Equilibrium shear modulus
C_{FG}	J kg^{-1} K^{-1}	Specific heat capacity at a fixed state of deformation in the glassy state. This constant weights a term that produces a linear response with respect to temperature
α_G	K^{-1}	Non-equilibrium volumetric thermal expansion coefficient
β^G	none	Non-equilibrium volumetric deformation associated with the chemical reaction extent
η_{rxnG}	J m^{-}3	Non-equilibrium entropy density (per unit reference volume) associated with the thermal chemistry
f^i	none	Relaxation process associated with the ith reaction
τ_i	s	Stretched exponential time constant associated with the ith spectrum
γ_i	none	Stretched exponent associated with the ith spectrum
C_1	none	Viscoelastic clock parameter associated with temperature
C_2	K	Viscoelastic clock parameter associated with temperature
C_3	K	Viscoelastic clock parameter associated with volume deformation
C_4	K	Viscoelastic clock parameter associated with shear deformation

Table 3.3. Non-equilibrium helmholtz free energy density parameters.

Chapter 4

Results

Recall that the objective of this paper is to examine the difference in thermal-mechanical behavior between removable and traditional thermosetting encapsulations, and so we focus on scenarios in which the temperature field is controlled. Furthermore, since we neglect species diffusion, we may focus only on balancing momentum as the material is subjected to different thermal-mechanical boundary value problems. Thus, we implement the constitutive model into Sandia's Library for Advanced Materials in Engineering (LAME) and run simulations using Sierra/SM, an implicit, quasi-static finite deformation momentum balance code. Simulations use 3D linear hexahedral finite elements with a selective deviatoric integration scheme. Through its implementation in LAME, the model may be linked with in-house Sandia energy balance and species diffusion codes to fully represent transient thermal-chemical-mechanical analysis if necessary. We present three sets of results with associated objectives:

- We develop a (semi-)analytic solution to an applied uniaxial deformation and thermal history of the removable polymer model under equilibrium chain conditions. These results showcase the network relaxation behavior due to the Diels-Alder chemistry without the added complexity the non-equilibrium viscoelasticity.
- We calibrate and validate the constitutive model against data in the literature to show its predictive capabilities.
- We contrast the behaviors of a removable vs. non-removable thermosetting polymers in encapsulation scenarios. These results have important ramifications on the use of removable polymers in electronics packaging.

Analytic Solutions of Rubbery Removable Encapsulation

Our objective is to determine the thermal-chemical-mechanical behavior of the removable polymer model when we subject a material point to an applied uniaxial stress and temperature history. Immediately, we neglect the non-equilibrium viscoelastic behavior discussed in section 3 as well as any volume change associated with evolving the extent of reaction ($\beta = 0$ in Eq. 3.62). Consider the scenario in which we apply a strain history in the 11 direction ($\Upsilon_{11} = \Upsilon_{11}\left[t\right], t \geq 0$) while the other two principal directions remain traction free ($S^{\Upsilon}_{22} = S^{\Upsilon}_{33} = 0, t \geq 0$). We focus on the stress work conjugate to the logarithmic strain, Eq. 3.62, which can be transformed to the Second Piola-Kirchoff stress via Eq. 3.21 as desired. We seek to compute the axial stress, ($S^{\Upsilon}_{11}[t]$), the transverse strain ($\Upsilon_{22}[t] = \Upsilon_{33}[t]$), and the permanent axial and transverse strains that arises from the Diels-Alder chemistry and network rearrangement ($\xi_{11}[t], \xi_{22}[t] = \xi_{33}[t]$). Requiring that the transverse stresses are zero, one may solve for the transverse strain as a function of time from Eq. 3.62,

$$\Upsilon_{22} = \left(\frac{K\alpha^{\infty}(\Theta - \Theta_{ref})}{2} + \left(\frac{G^{\infty}}{3} - \frac{K}{2}\right)\Upsilon_{11} + G^{\infty}\xi_{22}\right)\left(\frac{G^{\infty}}{3} + K\right)^{-1}. \tag{4.1}$$

The permanent deformation evolves from Eq. 3.54, such that the transverse component obeys,

$$\dot{\xi}_{22} = \frac{\dot{G}^{\infty}_{+}}{3G^{\infty}}\left(\frac{K(\alpha_{\infty}(\Theta - \Theta_{ref}) - 3\Upsilon_{11})}{2(\frac{G^{\infty}}{3} + K)} + \xi_{22}\left(\frac{G^{\infty}}{\frac{G^{\infty}}{3} + K} - 3\right)\right). \tag{4.2}$$

Since the permanent strain tensor, ξ_{ij} is deviatoric by construction (see Eq. 3.54), the permanent axial deformation is $2\xi_{11} = -\xi_{22}$. If Eq. 4.2 can be integrated, then the permanent deformation tensor and total logarithmic strain tensors are known (the latter via Eq. 4.1), and consequently, the axial stress can be obtained from Eq. 3.62. However, Eq. 4.2 is difficult to integrate under arbitrary applied axial strain and temperature histories because, as they change, chemical equilibrium changes in accordance with Eqs. 3.34 and 3.35, and so the equilibrium shear modulus (G^{∞}) changes via 3.48 along with the rate of increase of the shear modulus ($\dot{G}^{\infty}_{+}$) due to the forward Diels-Alder reaction (Eqs. 3.50 and 3.51).

If we further restrict ourselves to isothermal conditions, then the system is in chemical equilibrium, and G^{∞}, G^{∞}_{+}, and $\alpha_{\infty}(\Theta - \Theta_{ref})$ are all constants. Then, Eq. 4.2 can be integrated for certain applied axial strain histories. Consider an isothermal, uniaxial stress relaxation scenario in which the applied axial strain history is $\Upsilon_{11} = \bar{\Upsilon}, \quad t \geq 0$. The corresponding transverse permanent strain from Eq. 4.2 is,

$$\xi_{22} = -\frac{a}{b}\left(1 - \exp[-bt]\right), \tag{4.3}$$

$$a = \frac{\dot{G}^{\infty}_{+}}{3G^{\infty}}\left(\frac{3\bar{\Upsilon} - \alpha^{\infty}(\Theta - \Theta_{ref})}{2(\frac{G^{\infty}}{3} + K)}\right)K, \quad b = \frac{\dot{G}^{\infty}_{+}}{3G^{\infty}}\left(3 - \frac{G^{\infty}}{\frac{G^{\infty}}{3} + K}\right).$$

The total transverse strain can be computed from Eqs. 4.1 and 4.3, and finally, the axial stress may be computed straightforwardly from Eq. 3.62.

The main result from the isothermal stress relaxation boundary value problem is the exponential evolution of the the transverse strain, permanent strain, and axial stress. Since there is only one time scale, which is set by $\frac{G^{\infty}}{\dot{G}^{\infty}_{+}}$, a single set of results characterizes isothermal, rubbery stress relaxation due to network topology evolution if Fig. 4.1. As thermal expansion only serves to offset the initial

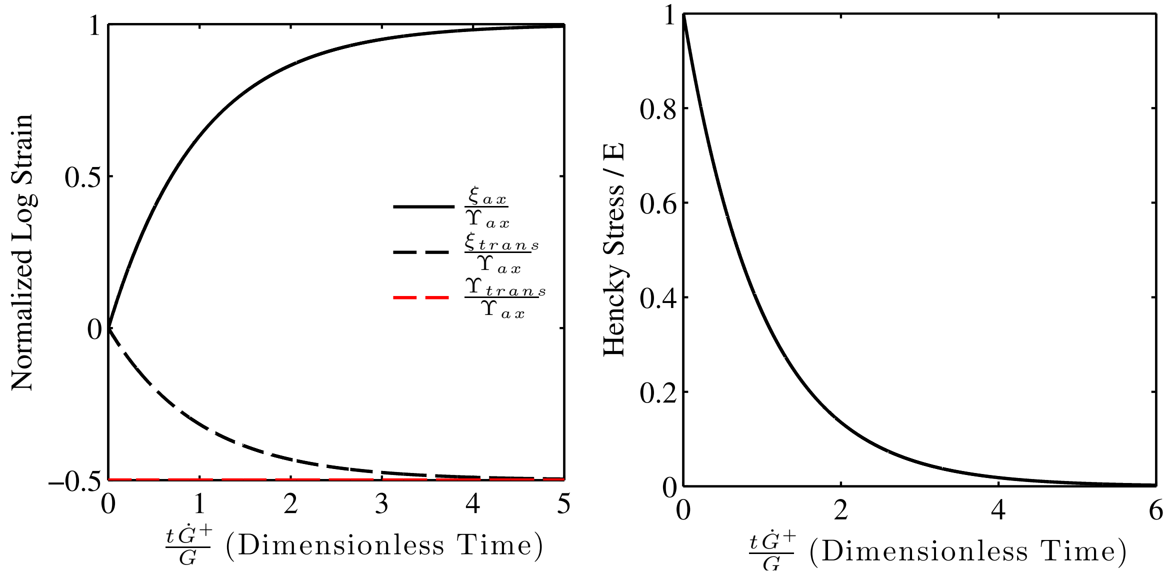

(a) Stress free (ξ_{ij}) and transverse log strains (Υ_{trans}) normalized to the applied log strain (Υ_{ax}).

(b) Axial stress normalized by Young's Modulus

Figure 4.1. Analytic solution of an RNP subjected to an isothermal, stress relaxation protocol in its rubbery state. Thermal expansion is neglected without loss of solution generality. A sudden logarithmic strain of 1 is applied at $t = 0$, and the ratio of the bulk to shear moduli is 10^6 corresponding to the nearly incompressible limit of elastomers.

applied deformation, it is neglected in these analytic results. From Fig. 4.1(b), the axial stress in the material approaches zero after a sufficient amount of dimensionless time. For the stress tensor to be zero, both the deviatoric and volumetric contributions must vanish, which is exactly what the evolution of the stress free strain tensor accomplishes in Fig. 4.1(a). The stress decays because the permanent shape of the material evolves to become the deformed shape. An interesting feature of this process is that the stress free strain tensor is by construction deviatoric, and so we see the relaxation of elastic volumetric deformation due to the removable of deviatoric stresses. Another interesting feature of this result is that regardless of the ratio of bulk to shear moduli, the zero stress state is the same, and so all solutions will arrive at the permanent deformations in Fig. 4.1(a) although their initial trajectories may differ.

Isothermal uniaxial extension at a constant logarithmic strain rate is also modeled analytically. Here, the applied axial strain is given by $\Upsilon_{11} = \dot{\Upsilon}t, \quad t \geq 0$, where $\dot{\Upsilon}$ is a constant. The associated permanent transverse logarthmic strain can be integrated from Eq. 4.1,

$$\xi_{22} = \frac{(a-bc)(1-\exp[-bt])-abt}{b^2}, \tag{4.4}$$

$$a = \frac{\dot{G}_+^\infty}{3G^\infty}\left(\frac{3\dot{\Upsilon}K}{2(\frac{G^\infty}{3}+K)}\right), \quad b = \frac{\dot{G}_+^\infty}{3G^\infty}\left(3-\frac{G^\infty}{\frac{G^\infty}{3}+K}\right),$$

$$c = -\frac{\dot{G}_+^\infty}{3G^\infty}\left(\frac{\alpha^\infty(\Theta-\Theta_{ref})}{2(\frac{G^\infty}{3}+K)}\right)$$

Again, the total transverse logarithmic strain and axial stress can be computed from Eqs. 4.1 and 3.62 respectively using Eq. 4.4. In contrast to the sudden isothermal stress relaxation problem, there are two time scales in the isothermal, uniaxial extension scenario, one associated with the strain rate, $\dot{\Upsilon}$, while the other is associated with the rate of permanent shape change due to network topology evolution, $\frac{\dot{G}_+^\infty}{G^\infty}$. The ratio of these time scales determines the model's response, $\frac{\dot{\Upsilon}G^\infty}{\dot{G}_+^\infty}$, which is shown for different ratios in Fig. 4.2.

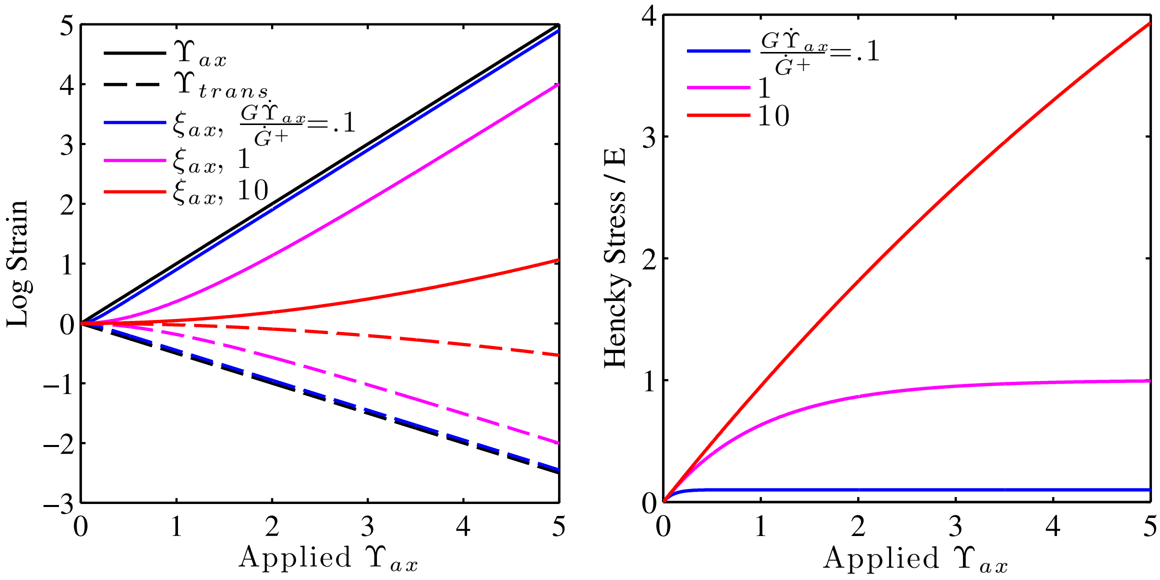

(a) Stress Free Strains (ξ_{ij}) **(b)** Axial Stress

Figure 4.2. Analytic solution of an RNP subjected to an isothermal, constant logarithmic strain rate uniaxial extension protocol in its rubbery state. The axial and transverse strains are provided and represent the limit when the strain rate is much faster than the relaxation rate due to network topology evolution. Thermal expansion is neglected without loss of solution generality. the ratio of the bulk to shear moduli is 10^6 corresponding to the nearly incompressible limit of elastomers.

There are two clear limiting regimes. If $\frac{\dot{\Upsilon}G^\infty}{\dot{G}_+^\infty} >> 1$, then there is no significant evolution to the network topology, and so the model exhibits a linear elastic response as expected. On the other hand, if $\frac{\dot{\Upsilon} G^{\infty}}{\dot{G}^{\infty}_{+}} << 1$, then the evolution of the network topology and associated stress relaxation rate is much faster than the strain rate. Hence, the material ”flows” with applied deformation and no stress is produced. When these two rates are comparable, as is the case in Fig. 4.2, then a steady state behavior is set by the ratio itself. Specifically, the maximum axial stress (normalized by Young’s modulus) approaches this ratio, which can be clearly seen in Fig. 4.2(b) for the values of $\frac{\dot{\Upsilon} G^{\infty}}{\dot{G}^{\infty}_{+}} = 0.1, 1$.

Model Calibration and Validation

We turn our attention towards validating the model’s predictive capability to simulate the polymer dynamics associated with the Diels-Alder chemistry/stress relaxation behavior of RNPs. Our objective is to predict the dynamic mechanical analysis (DMA) behavior of a specific RNP from [6], which is a challenging task because it involves three time scales: non-linear viscoelastic glassy behavior, DA chemistry and associated network relaxation, and the time scale of mechanical perturbation. Furthermore, it sweeps a range of temperatures and perturbation frequencies. The DMA protocol involves isothermal frequencies sweeps in oscillatory shear.

Since the DMA experimental data is isothermal and least 25C more above the glass transition, we consider only a rubbery RPM model calibration, which includes the DA chemistry/network relaxation but has turned off all viscoelastic behavior and thermal properties. This version of the model can be fully calibrated from chemical and mechanical data from reference [6] without any adjustable parameters. Mechanically, we select one rubbery shear modulus value at 75C, and choose the bulk modulus to be 4 orders of magnitude larger to replicate nearly incompressible elastomeric behavior. The chemical and rubbery model parameters are summarized in table 4.1. Unfortunately, insufficient experimental data existed in the work of Bowman and co-workers to populate the glassy behavior of the RPM model; so we could not include such behavior in this validation study.

Θ_{ref}	75C	x_{gel}	$\frac{1}{\sqrt{2}}$
K^{∞}	3.8e8 Pa	G^{∞}_{ref}	3.8e4 Pa
D^{α}	0 m^2 s^{-1}	β^{∞}	0
ΔH°_{rxn}	-400 J mol^{-1}	$\Delta \eta^{\circ}_{rxn}$	-106 J K^{-1}
k_0	5.6e9 s^{-1}	E_{act}	88e4 J

Table 4.1. Calibrated material properties associated with the dynamic mechanical analysis validation predictions. Quantities are taken directly from reference [6] with the exception of K^{∞} and β^{∞}, which were chosen as discussed in the text.

Clearly, the experimental data can be divided into two regimes dominated by chemical relaxation and one in which viscoelasticity begins to play a role. In the former regime, the RPM model

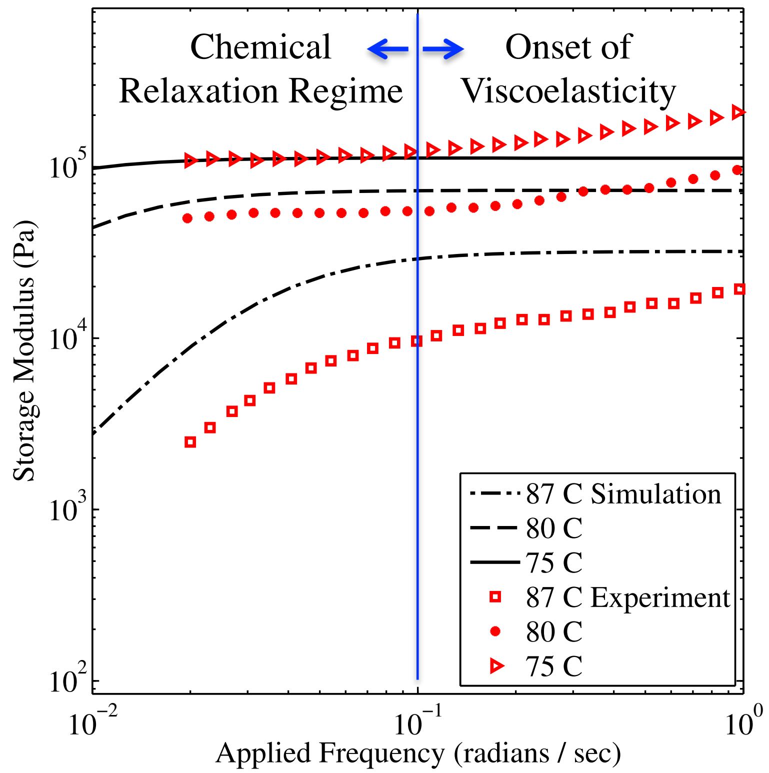

Figure 4.3. Comparison between model predictions and experiments in dynamic mechanical analysis under oscillatory shear. Storage shear moduli are presented for three isothermal frequency sweeps. Data is reproduced from reference [6]. The line that distinguishes between chemical relaxation and the onset of viscoelasticity is meant to qualitatively divide these two behavior regimes.

with no adjustable parameters reasonably captures the qualitative behavior of the experimental system. At slower frequencies and higher temperatures, the rate of network topology evolution (permanent shape change) is so fast that the material essentially “flows” with the applied deformation and cannot store elastic energy. Clearly, the model is not quantitatively accurate especially at the highest temperature. Note that 87C is very close to the gel point transition, and this close to the percolation threshold, the principal of rheological simplicity may not hold and/or the linear dependence of the shear modulus with respect to extent of reaction may not be accurate.

In the middle, especially for the 78 and 80C curves, both the experiment and model demonstrate similar rubbery plateau’s in which the storage modulus is less sensitive to frequency on a given isotherm. This result make sense in the context of the rubbery RPM model. Without viscoelasticity, only two time scales are active, and if the applied mechanical time scale is much faster than the chemistry/network topology evolution, then the network behaves in an elastic manner; hence the model produces a distinct rubbery plateau at sufficiently fast frequencies for each temperature.

Finally, at the fastest frequencies, while the RPM model continues on its rubbery plateau, the experimental data are showing the onset of the viscoelastic time scale (the onset of glassy behavior). Of course, this part of the model was not calibrated due to a lack of necessary data, but clearly the experimental trend–and the model capability to represent it–is consisent with expectations from the time-temperature superposition principal.

Removable Thermosets in Underfill Scenarios

The objective of this section is to distinguish the behavior of RNP and traditional thermoset encapsulations in relevant thermal-mechanical scenarios. We are particularly interested in underfill applications wherein an encapsulation's thermal-mechanical behavior may strongly influence the conditions for solder-joint fatigue (See Fig. 2.1) due to the large thermal expansion mismatch of the polymer underfill and neighboring ceramic and metallic components. Clearly, the RNP is beneficial/detrimental compared with traditional thermoset encapsulation if it experiences lower/higher stresses during thermal cycling, which ultimately are applied to surrounding components. To make this comparison, we examine a simple, homogenous motion, single element boundary value problem in which the displacement field is constrained along one axis while the other two axes unconstrained (and their outward surfaces are traction free), which may primitively represent underfill scenarios (neglecting adhesion constraints at the interfaces). This element is subjected to a thermal cycle representative of taking a material from a post-cured state at an elevated temperature, holding it at an intermediate temperature, and then cycling the temperature. The applied temperature field used is provided.

The behavior of the removable network polymer model is determined by three competing time scales:

- The experimental time scale associated with the rates of applied deformation and temperature change
- Chemical kinetics, such as the half-life of a Diels-Alder linkage
- The non-linear viscoelastic time scale ($\frac{1}{a}$)

The analytic solutions in section 4 dealt only with the first two time scales under special conditions in which they are fixed. However, in encapsulation scenarios, materials are subjected to thermal cycles in which all three time scales vary. If the material is in the glassy state throughout the entire thermal cycle, then the model will predict no significant network topology evolution based on our assumption that chemical and viscoelastic kinetics act in parallel in influencing the rate of shape change (see Eq. 3.47), and so we do not observe differences between removable and traditional encapsulation under that condition. However, if the glass transition occurs within or below the thermal cycle temperature range, then differences will arise.

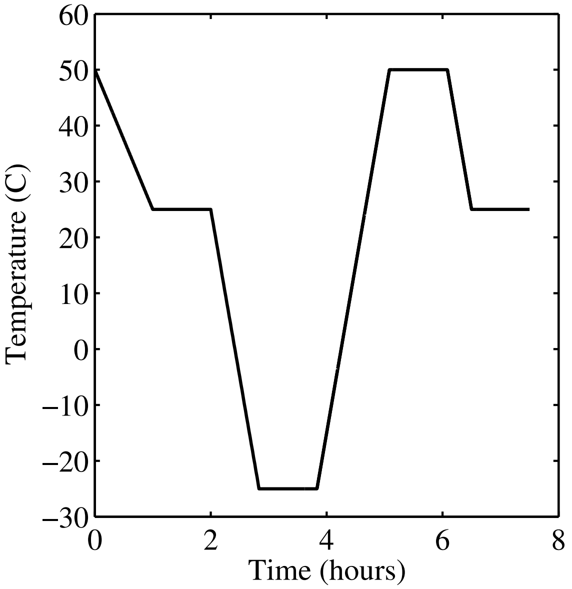

Figure 4.4. Temperature history applied in the simple, homogenous motion, uniaxial stress encapsulation scenario.

We consider two scenarios, one in which Θ_{glass} is equal to the minimum temperature in the thermal cycle (-25C) and the other in which Θ_{glass} is in the middle of the thermal cycle. For these analyses, we choose a different encapsulation material, namely an epoxy thermoset (828 DEA) that has been extensively studied and characterized for encapsulation applications . To compare it to the model in this paper, we simply "turn-on" the additional thermal-chemistry and consider that the RPM's rubbery properties are calibrated to 25C instead of 75C. To examine the role of vitrification, we change the reference temperatures of the glass transition between the two scenarios. A table of the system parameters for each scenario is reported in table 4. In the first scenario, $\Theta_{glass} = \Theta_{min}$ from Fig 4.4, so that the materials are in the rubbery state the whole time. Note that, although we change the temperature now, we are focused on the mechanical response, and so we neglect thermal properties.

The removable and traditional thermosets differ in their axial stress responses in Fig. 4.6 due both to the changing stress free configuration of the removable thermoset as seen in Figs. 4.6(a) and 4.6(d) as well as the non-linear temperature dependence of its rubbery shear modulus; by contrast, the rubbery shear modulus of the traditional thermoset does not change substantially over the temperature range. Recall that the RPM models the rubbery shear modulus with a linear dependence on temperature and the extent of reaction (Eq. 3.48), which itself (at equilibrium) depends exponentially on the temperature through the equilibrium constant (Eq. 3.34). Indeed, in this scenario, the extent of reaction changes from approximately 0.86 to 0.89, which corresponds to a 20% change in rubbery shear modulus relative to the $\frac{1}{\sqrt{2}}$ gel point extent of reaction! Moreover, the extent of reaction is often not in equilibrium, which, at the lowest temperature of -25C would be approximately 0.98 with the thermal-chemical constants in table 4 and the equilibrium constant

Θ_{ref}	25C	x_{gel}	$\frac{1}{\sqrt{2}}$
K^{∞}	3.2e9 Pa	G_{ref}	4.5e6 Pa
K_{glass}	4.9e9 Pa	G_{glass}	0.9e9 Pa
D^{α}	0 m^2s^{-1}	β^{∞}	0
ΔH°_{rxn}	-40 $kJmol^{-1}$	$\Delta\eta^{\circ}_{rxn}$	-106 $Jmol^{-1}K^{-1}$
k_0	5.6e9s^{-1}	E_{act}	88e4 J
α_{∞}	600 ppm K^{-1}	α_{glass}	170 ppm K^{-1}
C_1	16.5	C_2	54.5 K
C_3	1000 K	C_4	11800 K
τ_1	6 s	γ_1	0.24
τ_2	0.12 s	γ_2	0.22
Number of Proney Terms	17	Θ_{glass}	-25C, 25C

Table 4.2. Properties used in the two thermal mechanical simulations that compare removable vs. conventional thermosets. The proney terms are logarithmically spaced evenly between 10^-8 and 10^8 seconds. Two Proney series are fit in a least squares sense to the stretched exponential relaxation curves defined by (τ_1,γ_1), (τ_2,γ_2) in Eq. 3.67. Viscoelastic parameters were taken from [5]. Thermal-chemical constants were taken from [6].

equation 3.34. However, the chemical kinetics are sluggish at such low temperatures (see Fig. 2.1(b) for the half-life of a reversible linkage vs. temperature), which prevents the equilibrium state from being reached even in the absence of vitrification. Another important observation is that at the high temperature state, while the traditional thermoset returns to a zero stress state, the RPM predicts that the material responds in compression. This results is sensible since during the cooling process, the permanent shape of the removable thermoset changed to eliminate the tensile thermal eigenstrain.

In the second scenario, the glass transition is assumed to occur in both materials at 25C, which is in the middle of the thermal cycle. Vitrification plays a dominant role, and the material responses are only slightly distinguishable with respect to the axial stress response. In this scenario, the viscoelastic shift factor transitions from rubbery to glassy regimes and is almost identical between the two materials. While the initial cooling response produces a different stress response as with the previous scenario, this difference is negligible compared with the glassy response on further cooling until both materials cross above the glass transition temperature again. The effects of vitrification can also clearly be seen on the evolution of the permanent shape of the RPM material, which ceases below the glass transition in Fig. 4.6(d). However, in accordance with the model, the thermal-chemistry is limited only by its own kinetics as in the previous scenario.

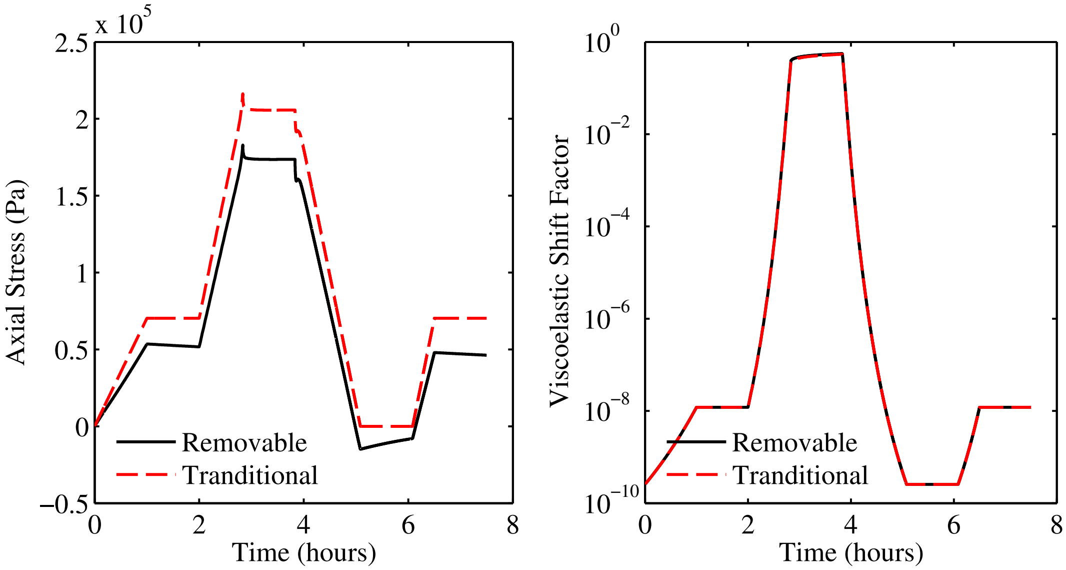

(a) Axial stress: $\Theta_{glass} = -25C$ **(b)** Viscoelastic shift factor: $\Theta_{glass} = -25C$

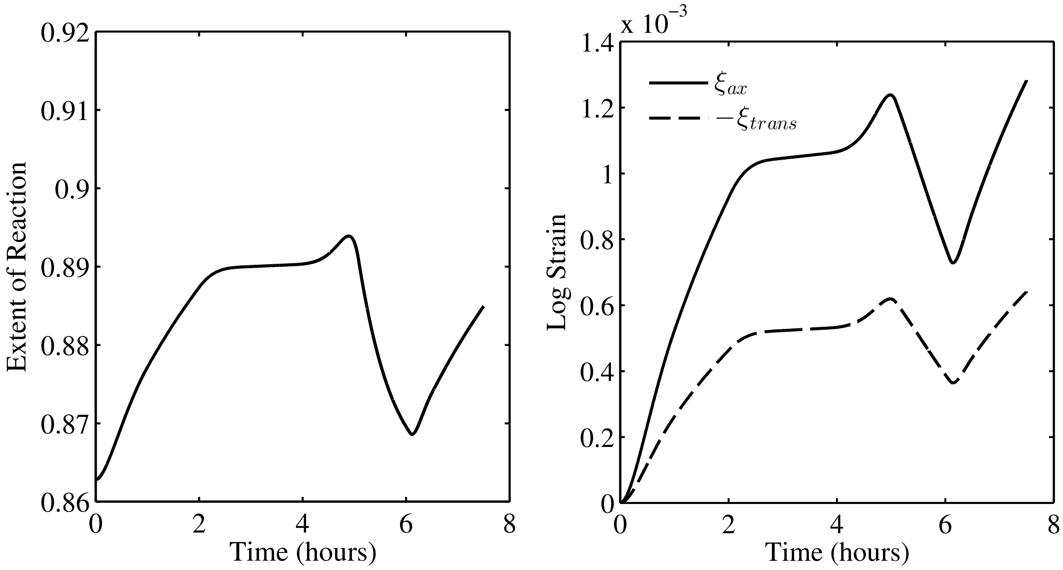

(c) Extent of reaction: $\Theta_{glass} = -25C$ **(d)** Permanent logarithmic strains: $\Theta_{glass} = -25C$

Figure 4.5. Single element encapsulation scenario in which $\Theta_{glass} = \Theta_{min}$ from Fig 4.4. Along one axis, the displacement field is fixed while traction free conditions are applied to the outer surfaces in the orthogonal directions. In this scenario, both materials remain rubbery throughout the thermal cycle, and a substantial difference in the axial stress response is observed between the two materials.

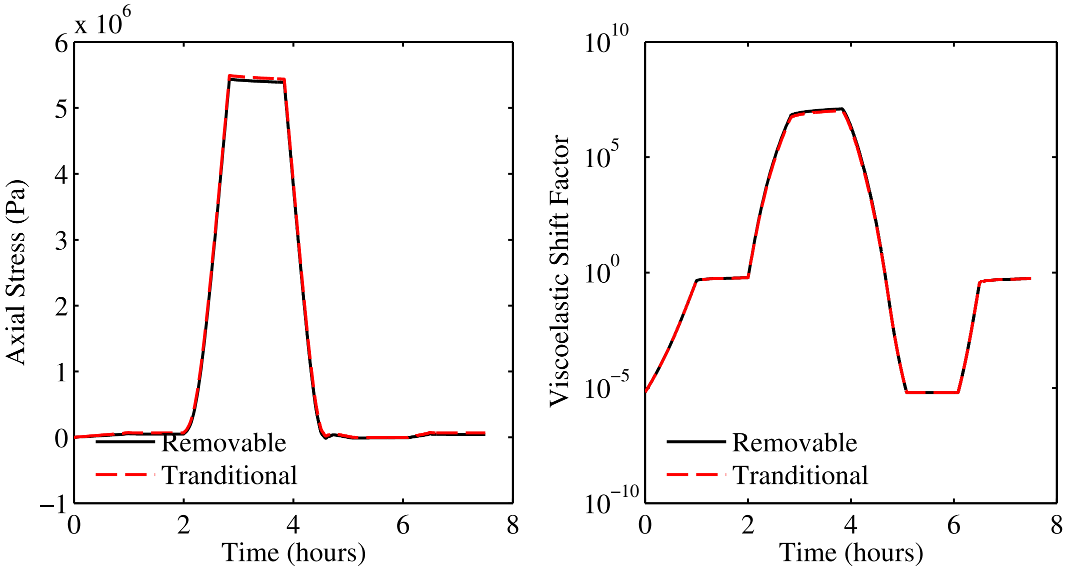

(a) Axial stress: $\Theta_{glass} = 25C$ **(b)** Viscoelastic shift factor: $\Theta_{glass} = 25C$

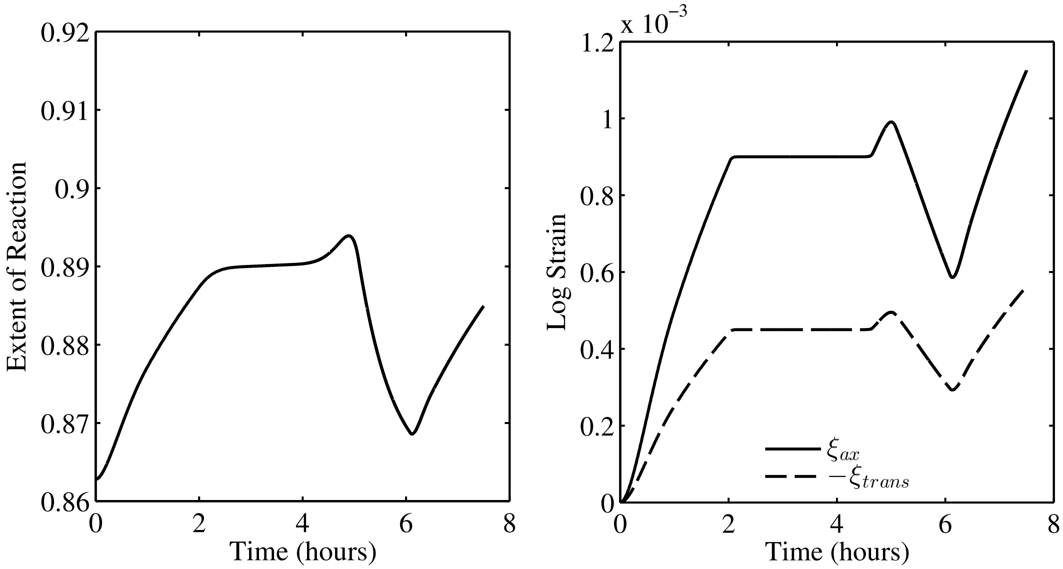

(c) Extent of reaction: $\Theta_{glass} = 25C$ **(d)** Permanent logarithmic strains: $\Theta_{glass} = 25C$

Figure 4.6. Single element encapsulation scenario in which $\Theta_{glass} = \Theta_{room}$ (25 C) from Fig 4.4. Along one axis, the displacement field is fixed while traction free conditions are applied to the outer surfaces in the orthogonal directions. In this scenario, each material transitions from a rubber to a glass as evidenced by the viscoelastic shift factor, and only a very small difference is observed between their stress responses.

Chapter 5

Conclusions

Thermosetting polymers with thermally reversible functionalities exhibit permanent shape change (stress relaxation) in the gelled state and a clear gel-point transition, above which the thermoset behaves in as a viscous liquid. Both of these intrinsic properties are distinct from conventional thermosets. The consequence of this gel point transition is that these thermosets can be removed. The focus of this paper has been to modeling the solid-like behavior of such removable network polymers (in their gelled states). Three time scales determine the thermal-chemical and mechanical responses of such materials:

- The rate of applied temperature change and/or deformation
- The kinetics of the reversible Diels-Alder reaction
- The viscoelastic time scale associated with the material's glassy polymer dynamics

Without any tuning parameters, the model for such materials validated reasonably well compared with limited experimental data, which suggests that at least qualitatively, the polymer dynamics for such materials are adequately represented by the work in this paper.

An objective of this work is to distinguish the thermal-mechanical behaviors of removable network polymers and traditional (non-removable) network polymers. Simulations in this article demonstrate that if viscoelasticity dominates the thermal-mechanical cycles, the two classes of materials respond identically. Also, if the thermal-mechanical conditions are such that vitrification is avoided and the rates of applied deformation and temperature change are considerably faster than the Diels-Alder chemical kinetics, then removable and traditional network polymers will behavior similarly as elastomers. However, given that the number density of chains, and therefore the rubbery shear modulus, evolves with temperature for removable network polymers, their thermal-mechanical behavior will be distinct even if network topology evolution is largely avoided.

However, if vitrification is either fully or partially avoided in the applied thermal-mechanical cycles, and the rates of mechanical and thermal stimuli are slow or comparable to the Diels-Alder chemical kinetics (and associated network topology evolution), then removable network polymers may behave in a significantly different manner compared with traditional thermosets. Given enough time, they can change their shape to become stress free in any configuration that does not involve volumetric deformation, and this has important ramifications on the use of such materials to mitigate cure shrinkage stresses and for use as encapsulation in electronics packaging.

References

[1] D. Adolf and J. E. Martin. Time cure superposition during cross-linking. *Macromolecules*, 23(15):3700–3704, 1990.

[2] D. Adolf, S. Spangler, K. Austin, M. Neidigk, M. K. Neilsen, and R. S. Chambers. Packaging strategies for printed circuit board components volume i materials and thermal stresses. *SANDIA REPORT Unlimited Release*, SAND4751:1–114, 2011.

[3] D. B. Adolf and R. S. Chambers. A thermodynamically consistent, nonlinear viscoelastic approach for modeling thermosets during cure. *Journal of Rheology*, 51(1):23–50, 2007.

[4] D. B. Adolf, R. S. Chambers, and J. M. Caruthers. Extensive validation of a thermodynamically consistent, nonlinear viscoelastic model for glassy polymers. *Polymer*, 45(13), 2004.

[5] D. B. Adolf, R. S. Chambers, and M. A. Neidigk. A simplified potential energy clock model for glassy polymers. *Polymer*, 50(17):4257–4269, 2009.

[6] B. J. Adzima, H. A. Aguirre, C. J. Kloxin, T. F. Scott, and C. N. Bowman. Rheological and chemical analysis of reverse gelation in a covalently cross-linked diels-alder polymer network. *Macromolecules*, 41(23):9112–9117, 2008.

[7] B. J. Adzima, C. J. Kloxin, and C. N. Bowman. Externally triggered healing of a thermoreversible covalent network via self-limited hysteresis heating. *Advanced Materials*, 22(25):2784–+, 2010.

[8] R. D. Andrews, A. V. Tobolsky, and E. E. Hanson. The theory of permanent set at elevated temperatures in natural and synthetic rubber vulcanizates. *Journal of Applied Physics*, 17(5), 1946.

[9] J. M. Caruthers, D. B. Adolf, R. S. Chambers, and P. Shrikhande. A thermodynamically consistent, nonlinear viscoelastic approach for modeling glassy polymers. *Polymer*, 45(13), 2004.

[10] X. X. Chen, F. Wudl, A. K. Mal, H. B. Shen, and S. R. Nutt. New thermally remendable highly cross-linked polymeric materials. *Macromolecules*, 36(6):1802–1807, 2003.

[11] B. D. Coleman and M. E. Gurtin. Thermodynamics with internal state variables. *Journal of Chemical Physics*, 47(2):597, 1967.

[12] P. J. Flory. Elasticity of polymer networks cross-linked in states of strain. *Transactions of the Faraday Society*, 56(5):722–743, 1960.

[13] Qi Ge, Xiaofan Luo, Erika D. Rodriguez, Xiao Zhang, Patrick T. Mather, Martin L. Dunn, and H. Jerry Qi. Thermomechanical behavior of shape memory elastomeric composites. *Journal of the Mechanics and Physics of Solids*, 60(1), 2012.

[14] James H. Aubert James R. McElhanon, Edward M. Russick. Removable encapsulants. *SANDIA REPORT (Unlimited Release)–Science Matters!*, SAND5893:1–2, 2010.

[15] C. J. Kloxin, T. F. Scott, B. J. Adzima, and C. N. Bowman. Covalent adaptable networks (cans): A unique paradigm in cross-linked polymers. *Macromolecules*, 43(6):2643–2653, 2010.

[16] Christopher J. Kloxin, Timothy F. Scott, Hee Young Park, and Christopher N. Bowman. Mechanophotopatterning on a photoresponsive elastomer. *Advanced Materials*, 23(17), 2011.

[17] A. Lendlein, H. Y. Jiang, O. Junger, and R. Langer. Light-induced shape-memory polymers. *Nature*, 434(7035), 2005.

[18] K. N. Long, T. F. Scott, H. J. Qi, C. N. Bowman, and M. L. Dunn. Photomechanics of light-activated polymers. *Journal of the Mechanics and Physics of Solids*, 57(7):1103–1121, 2009.

[19] Kevin N. Long, Martin L. Dunn, and H. Jerry Qi. Mechanics of soft active materials with phase evolution. *International Journal of Plasticity*, 26(4), 2010.

[20] Kevin N. Long, Martin L. Dunn, Timothy F. Scott, Lucas P. Turpin, and H. Jerry Qi. Light-induced stress relief to improve flaw tolerance in network polymers. *Journal of Applied Physics*, 107(5), 2010.

[21] Kevin N. Long, Timothy F. Scott, Martin L. Dunn, and H. Jerry Qi. Photo-induced deformation of active polymer films: Single spot irradiation. *International Journal of Solids and Structures*, 48(14-15), 2011.

[22] J. E. Martin and D. Adolf. Constitutive equation for cure-induced stresses in a viscoelastic material. *Macromolecules*, 23(23):5014–5019, 1990.

[23] T. C. Mauldin and M. R. Kessler. Self-healing polymers and composites. *International Materials Reviews*, 55(6), 2010.

[24] J. R. McElhanon, E. M. Russick, D. R. Wheeler, D. A. Loy, and J. H. Aubert. Removable foams based on an epoxy resin incorporating reversible diels-alder adducts. *Journal of Applied Polymer Science*, 85(7):1496–1502, 2002.

[25] Damien Montarnal, Mathieu Capelot, Francois Tournilhac, and Ludwik Leibler. Silica-like malleable materials from permanent organic networks. *Science*, 334(6058), 2011.

[26] N. W. Polaske, D. V. McGrath, and J. R. McElhanon. Thermally reversible dendronized step-polymers based on sequential huisgen 1,3-dipolar cycloaddition and diels-alder ”click” reactions. *Macromolecules*, 43(3):1270–1276, 2010.

[27] K. R. Rajagopal and A. R. Srinivasa. Mechanics of the inelastic behavior of materials - part 1, theoretical underpinnings. *International Journal of Plasticity*, 14(10-11):945–967, 1998.

[28] D. R. Rottach, J. G. Curro, J. Budzien, G. S. Grest, C. Svaneborg, and R. Everaers. Molecular dynamics simulations of polymer networks undergoing sequential cross-linking and scission reactions. *Macromolecules*, 40(1):131–139, 2007.

[29] Jennie Ryu, Matteo D'Amato, Xiaodong Cui, Kevin N. Long, H. Jerry Qi, and Martin L. Dunn. Photo-origami-bending and folding polymers with light. *Applied Physics Letters*, 100(16), 2012.

[30] T. F. Scott, A. D. Schneider, W. D. Cook, and C. N. Bowman. Photoinduced plasticity in cross-linked polymers. *Science*, 308(5728), 2005.

[31] J. A. Shaw, A. S. Jones, and A. S. Wineman. Chemorheological response of elastomers at elevated temperatures: Experiments and simulations. *Journal of the Mechanics and Physics of Solids*, 53(12), 2005.

[32] Richard J. Sheridan, Brian J. Adzima, and Christopher N. Bowman. Temperature dependent stress relaxation in a model diels-alder network. *Australian Journal of Chemistry*, 64(8), 2011.

[33] M. L. Szalai, D. V. McGrath, D. R. Wheeler, T. Zifer, and J. R. McElhanon. Dendrimers based on thermally reversible furan-maleimide diels-alder adducts. *Macromolecules*, 40(4):818–823, 2007.

[34] Mehmet Atilla Tasdelen. Diels-alder "click" reactions: recent applications in polymer and material science. *Polymer Chemistry*, 2(10), 2011.

[35] A. S. Wineman and J. A. Shaw. Scission and healing in a spinning elastomeric cylinder at elevated temperature. *Journal of Applied Mechanics-Transactions of the Asme*, 69(5), 2002.

[36] H. H. Winter. Can the gel point of a cross-linking polymer be detected by the g – g crossover? *Polymer Engineering Science*, 27(22):1698–1702, 1987.

[37] Rudy J. Wojtecki, Michael A. Meador, and Stuart J. Rowan. Using the dynamic bond to access macroscopically responsive structurally dynamic polymers. *Nature Materials*, 10(1), 2011.

DISTRIBUTION:

1	MS 1303	Gary S. Grest, 1131
1	MS 0834	Duane B. Dimos, 1500
1	MS 0346	Anne Grillet, 1512
1	MS 0346	Lisa A. Mondy, 1512
1	MS 0346	Christine C. Roberts, 1512
1	MS 0836	Rekha R. Rao, 1514
1	MS 0836	Scott A. Roberts, 1514
1	MS 0840	Justine E. Johannes, 1520
1	MS 0372	Nicole L. Breivik, 1524
1	MS 0372	Edmundo Corona, 1524
1	MS 0824	James Cox, 1524
1	MS 0372	Kristin Dion, 1524
1	MS 0372	John M. Emery, 1524
1	MS 0372	Huei Eliot Fang, 1524
1	MS 0372	Jhana Gorman, 1524
1	MS 0372	Spencer Grange, 1524
1	MS 0372	Kenneth W. Gwinn, 1524
1	MS 0372	Terry D. Hinnerichs, 1524
1	MS 0372	Jacob Koester, 1524
1	MS 0372	Chi S. Lo, 1524
1	MS 0372	Kevin N. Long, 1524
1	MS 0372	Kurt E. Metzinger, 1524
1	MS 0346	E. David Reedy, 1524
1	MS 0372	William M. Scherzinger, 1524
1	MS 0840	Jose G. Arguello, Jr., 1525
1	MS 0840	Joseph E. Bishop, 1525
1	MS 0840	Timothy J. Fuller, 1525
1	MS 0372	Jeffrey D. Gruda, 1525
1	MS 0840	Pania Newell, 1525
1	MS 0840	John Pott, 1525
1	MS 0346	Robert S. Chambers, 1526
1	MS 0346	Brenton Elisberg, 1526
1	MS 0346	Matthew Neidigk, 1526
1	MS 1398	Michael K. Neilsen, 1526
1	MS 0346	Diane E. Peebles, 1526
1	MS 0372	Douglas Vangoethem, 1526
1	MS 0892	David R. Wheeler, 1714
1	MS 0888	James R. McElhanon, 1821
1	MS 0888	Edward M. Russick, 1821

1	MS 0359	Donna L. Chavez, 1911
1	MS 0958	Michael J. Kelly, 1833
1	MS 0958	Jamie M. Kropka, 1833
1	MS 0958	Jason J. Sharkey, 1833
1	MS 0958	Marke E. Stavig, 1833
1	MS 9042	James W. Foulk III, 8256
1	MS 9042	Alejandro Mota, 8256
1	MS 9042	Jakob Ostien, 8256
1	MS 0899	Technical Library, 9536 (electronic copy)

Sandia National Laboratories